Dynamic Positioning using Integrator-Backstepping

- a non-linear Lyapunov stable observer-based approach

Rasmus L. Christensen
Master Thesis, Control and Automation
Department of Electronic Systems
Aalborg University

AD NYE VEJE
AALBORG UNIVERSITET

FORCE TECHNOLOGY

Dynamic Positioning using Integrator-Backstepping
- a non-linear Lyapunov stable observer-based approach

Preface

This thesis is handed in as partial fulfilment for the degree of Master of Science (MSc) in Engineering (Control and Automation) at Aalborg University, Section for Control and Automation. The thesis has been written in the period between the 2. Febuary and the 4. June. The oral defence will take place on the 23rd of June, 2014.

The project has been done in collaboration with FORCE TECHNOLOGY , who have provided data for the vessel, as well as a computer with the software simulating tool DEN-Mark1.

My supervisors through the project period have been Associate Professor, PhD Jan D. Bendtsen from Aalborg University, and PhD Michael Hansen from FORCE TECHNOLOGY . I would like to extend my gratitude towards them both for their guidance throughout the project period. A big thanks should also be given to my dad for nudging my head in a maritime inspired direction, as well as general discussions on the behaviour of ships.

The report is non-confidential, and all constants presented are normalized. The simulations and graphs are however carried out with the actual constants.

The report contains 87 pages including 3 appendices. 5 printed copies have been produced.

Aalborg, 04-06-2014

Rasmus Lundgaard Christensen

Abstract

This project documents the development of a non-linear controller, estimator and model to be used for dynamic positioning of a shuttle tanker. State-of-the-art methods have been developed by [FG98], which employs a backstepping framework for the control of a supply ship. This project is based on this work, and fosters to improve on the outcome, by including the wave induced motions in the stability analysis.

The estimator is based on the works of [FS99] who develops a wave filtering estimator that is both stable and passive in a Lyapunov sense. The estimator is based on the known non-linear model of the vessel, and through this, provides the controller with an estimate of the position that is better than using raw GPS and compass measurements. The estimator is shown to be exponentially globally stable, and will thus provide an estimate that over time converges to the true measurement. The stability properties and tuning of the filter is achieved using the Kalman-Yakubovich-Popov lemma.

The end result is a uniform globally exponential stable controller that is able to maintain the vessels position whilst under the influence of disturbances. The benchmark of the controller is the linear system used at FORCE TECHNOLOGY to test if various thruster configurations of ships are able to maintain the position under specified disturbances. Results have shown that the non-linear controller outperforms the linear counterpart, and as such could replace the system used at FORCE TECHNOLOGY .

Besides the controller, initial steps to develop an on-line thrust allocating module by solving a quadratic equation have been developed and tested, however, large jumps in the control signal makes the allocating module unstable. The complexity of the optimization problem is evident by the two azimuth thrusters mounted on the vessel, which both requires an angle and an input force, and through this, can be used to produce a force in the x- and y-direction as well as a moment about the z-axis.

To the authors knowledge, no one have included the wave induced motion parameter in the stability analysis of ships - and these findings make way for a deeper investigation into non-linear control of ships and other off-shore vehicles. Proposals to make the system even more robust are discussed in the report.

Resumé

Dette projekt dokumenterer udviklingen af en ikke-lineær controller, estimator samt model, til brug i dynamis positionering af en shuttle tanker. State-of-the-art metoder udviklet af [FG98], gør brug af backstepping metoder til kontrol af et forsynings skib. Denne rapport er baseret på dette arbejde, og foreslår en metode hvormed de forstyrrelser bølgerne inducerer på skibet kan inkluderes.

Estimatoren er baseret på [FS99], der har udviklet en bølgefiltrerende estimator der både udviser Lyapunov stabilitet samt passivitet. Estimatoren er baseret på den kendte ikke-lineære model af skibet, og gennem denne, udregnes estimater af skibets attitude til brug i controlleren. Estimatoren viser at kunne forbedre på GPS samt kompas målinger. Estimatoren vises at være eksponentielt global stabil, og vil derved give estimater der over tid konvergerer mod den sande måling. Stabilitets egenskaben samt tuningen af filtret sker ved brug af Kalman-Yakubovich-Popov lemmaet.

Slut resultatet er en uniform global eksponentiel stabil controller, der kan holde fartøjets position under indflydelse af eksterne forstyrrelser. Sammenligningsgrundlaget for controlleren er det lineære system der i øjeblikket anvendes hos Force Technology . Dette system bruges til at teste thruster-konfigurationer under en række givne forstyrrelser. Resultater viser at den ikke-lineære controller er bedre end dens lineære modstykke, og foreslåes derfor som udskiftning til det system der bruges hos Force Technology .

Udover controlleren, er start skridtet taget til at udvikle et on-line thrust allokerings modul, der løser en kvadratisk ligning, og gennem dette giver en optimal løsning på hvorledes de enkelte thrusters skal agere for at opnå den ønskede thrust. Store udsving i kontrol signalet har desværre vist at den foreslåede algoritme ikke kan håndtere store udsving i reference signalet. Kompleksiteten af problemet stammer fra de 2 azimuth thrustere der er monteret på skibet. Disse kan både producere en kraft i x- og y-retningen samt et moment omkring z-aksen, og allokeringen har således svært ved at finde en endelig løsning.

Umiddelbart er der ikke nogen der tidligere har forsøgt at inkludere den bølge baserede bevægelses parameter i stabilitets analysen for skibe, og dette forsøg lægger op til en større undersøgelse af ikke-lineær kontrol af skibe og andre off-shore fartøjer. Forslag der kan gøre systemet bedre bliver diskuteret i slutningen af rapporten.

Contents

List of Acronyms

CB Centre of Buoyancy.

CF Centre of Floatation.

CG Centre of Gravity.

CLF Candidate Lyapunov Function.

CO Centre of Origin.

DNV Det Norske Veritas.

DP Dynamic Positioning.

DWT Dead Weight Tonnes.

FPSO Floating Production Storage and Offloading.

GAS Globally Asymptotic Stable.

GES Globally Exponential Stable.

HIL Hardware-In-the-Loop.

RAO Response Amplitude Operator.

Chapter 1
Introduction

Throughout the last century, ships have been one of the primary methods of transporting goods and people between continents. From back when the Vikings roamed over Europe, to the large container ships sailing between Asia and America today, ships have been a big part of keeping the world going. Over the past two centuries, the study of ships and how they interact with the surrounding fluids have been the subject of much study.

With the discovery of large oil reservoirs beneath the sea floor, a new use for ships were found, and the birth of dynamic positioning algorithms were born.

Dynamic positioning algorithms have been used in the offshore industry since the late 50's, with the Cuss 1 being the first attempt at positioning a ship at sea. 4 rotatable thrusters combined with an underwater network of acoustic devices allowed the Cuss 1 to maintain a position within a radius of 180 metres [Bas61].

Today, dynamic positioning algorithms are used aboard a large variety of ships, from platform supply vessels to large fishing vessels and even some private yachts have such a system installed. This thesis however focuses on shuttle tankers, and their use of these algorithms. This thesis uses a shuttle tanker as an example, but the derived theory could apply to all vessels.

Shuttle tankers are primarily used to transport crude oil from the oil fields to the on-shore refineries, where pipe lines are to expensive or considered impossible to lay due to a rocky sea beds, coral reefs and so forth. The shuttle tankers are operating in three different "modes": shuttle, loading and offloading. This thesis focuses on the loading procedure, as this is carried out at sea and involves the vessel being connected to a loading bouy as depicted on figure 1.1. This operation is the most critical, as the ship is being exposed to all the environmental disturbances, whilst being connected to a flexible hose carrying the oil to the vessel.

In these operations, it is critical that the vessel does not deviate too much from the desired position, as damage to the hose or bouy could cause vast and irreversible environmental damages.

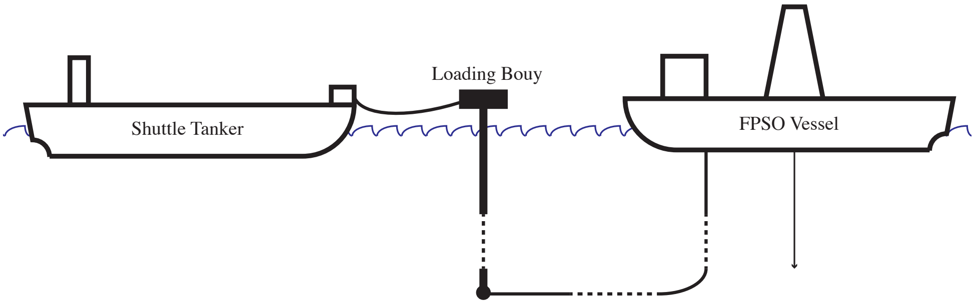

Figure 1.1: Illustration of the loading operation. The FPSO is connected to a seabed storage facility, where the vessel pumps its load aboard.

Over the years these control algorithms have improved as well as ship and thruster design. On the Cuss 1, the 4 outboards were manually configured, whereas the systems today are fully automatic. This also enforces stricter requirements to the vessels being outfitted with theses systems. To compare when the systems were first introduced to today, a list of requirements from Det Norske Veritas (DNV), [Ver12] to be certified "DPS2"-capable the vessel needs to fulfil the following hardware requirements:

- Redundancy in electrical systems.
- Redundancy in the power management system.
- Redundancy in thrusters.
- Have 2 computer systems aboard.
- Have 3 individual position reference systems.
- Have 2 wind sensors.
- Have 3 gyro compasses.
- Have 2 vertical reference units.
- Have 2 utility power supplies.

Compared to the Cuss 1 that was powered by 4 manually controlled outboard engines and one position reference system, the systems today are automated and are far more complex. This also calls for far more complex algorithms to interpret the measured data, react to the data compared to the desired position, compute thrust allocation, compute power allocation and be able to do this in most weather conditions.

On top of hardware requirements, DNV also certifies systems through software simulations. One such test is an Hardware-In-the-Loop (HIL) test. An HIL test, connects the dynamic positioning system to a simulator that simulates all the environmental conditions the ships might encounter, and the system response is analysed. If it meets certain criteria, the system is certified.

Hydrodynamic theory does however not account for all the constants related to the vessel, as some of the constants are hard to determine accurately. Hence scaled tests are carried out at FORCE TECHNOLOGY , to verify that a given thruster configuration can maintain the position through disturbances such as wind, currents and waves. A software simulation does however remove the need for producing a model of the vessel, and allows the ship owners to alter the design of the vessel at a smaller cost.

Currently FORCE TECHNOLOGY carries out model tests of ships, to verify to the ship owners that the vessels are able to maintain their position with a given thruster configurations and given environmental disturbances. These tests are time consuming, so the scope of this thesis will be to design an easy-to-tune system, that provides better responses that the system currently used.

Chapter 2
Analysis

To give an idea of the problem at hand, the current configuration used at FORCE TECHNOLOGY is analysed and improvements are suggested. Currently, the systems run at FORCE TECHNOLOGY consists of 3 independent linear PID controllers, a thruster lookup table and direct feedback of the measured signals. The tests are carried out by placing a scaled model of the vessel in the wave tank, and then having collinear disturbances perturb the vessel. This gives a worst-case answer of the control configuration. The angle of the disturbances are then changed, and the same test is carried out. This is done till the vessel cannot maintain the position, and from this, a maximum angle of attack can be established.

One of the primary reasons to update this system, is that control theory have come a long way since linear PID controllers, and employing a non-linear controller should provide better results as well as reduce the time spent tuning the controllers. Another benefit, is that once the model is developed a change in the angle of attack, does not influence the control law.

2.1 Current Control Configuration

The current control configuration is depicted on figure 2.1, a controller for x, y and ψ is used independently of one another. The thrust allocation module is a large lookup table computed before the tests, and the measured position and attitude is fed directly back to the control system with no noise cancellation or estimator used in between.

As the controllers are linearised around a working point $\boldsymbol{x}_0$, both linear and non-linear controllers should provide nearly the same answer close to this working point, however - further away, the difference will grow non-linearly, and the control signal will either be too large, too small or simply tend towards infinity. This is undesirable for ships in station keeping operations, as safety is a primary concern for ships at sea. The linear controller will provide a conservative estimate of the thruster

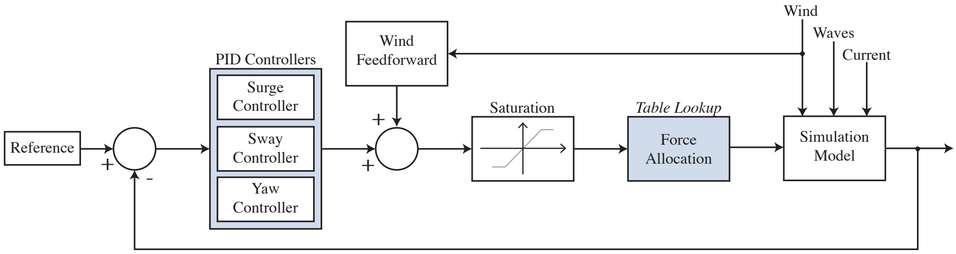

Figure 2.1: Illustration of the current control configuration used at FORCE TECHNOLOGY .

configurations ability to maintain position, and the actual ship should thereby be better than the test.

As the working point are are changed for each test, the controllers need re-tuning for every angle of attack. This is time consuming - and a way to ease this tuning process is desired.

2.2 Ship Primer

According to Encyclopaedia Britannica a ship is defined as:

Ship*: any large floating vessel capable of crossing open waters, as opposed to a boat, which is generally a smaller craft. The term formerly was applied to sailing vessels having three or more masts; in modern times it usually denotes a vessel of more than 500 tons of displacement. Submersible ships are generally called boats regardless of their size.*

The study of ships and their interaction with fluid have been a subject of research for a long time, and currently, no exact answer on their interaction with the fluid exists. Advances in fluid mechanics does however enable researchers to provide models that are accurate enough for use in control systems. The first simple studies of how ships interacted with the surroundings started around the industrial revolution in the 18th century to reduce the required thrust to move ships forward.

Nowadays, ships are generally mounted with one or two main propellers as the ships main propulsion as well as a rudder to manoeuvre the ship about. For ships that primarily operate in transit (cargo ships) this is sufficient, however, it is becoming increasingly common to mount bow and stern thrusters to increase manoeuvrability at low speeds, and to aid in docking operations. As the complexity of the operations the vessels undergoes increases, so does the complexity of the thrusters mounted. Many ships today are mounted with so-called azimuth thrusters. An azimuth thruster is able to rotate 360 degrees. The various thrusters are depicted on figure 2.2, where the leftmost thruster is the main propeller, the second from the left the tunnel thruster and the rightmost is the azimuth. The advantage of an azimuth thruster is that this can act as both a main thruster to provide forward (or backward) thrust, as well as be used to generate a moment about the z-axis of the ship in manoeuvring.

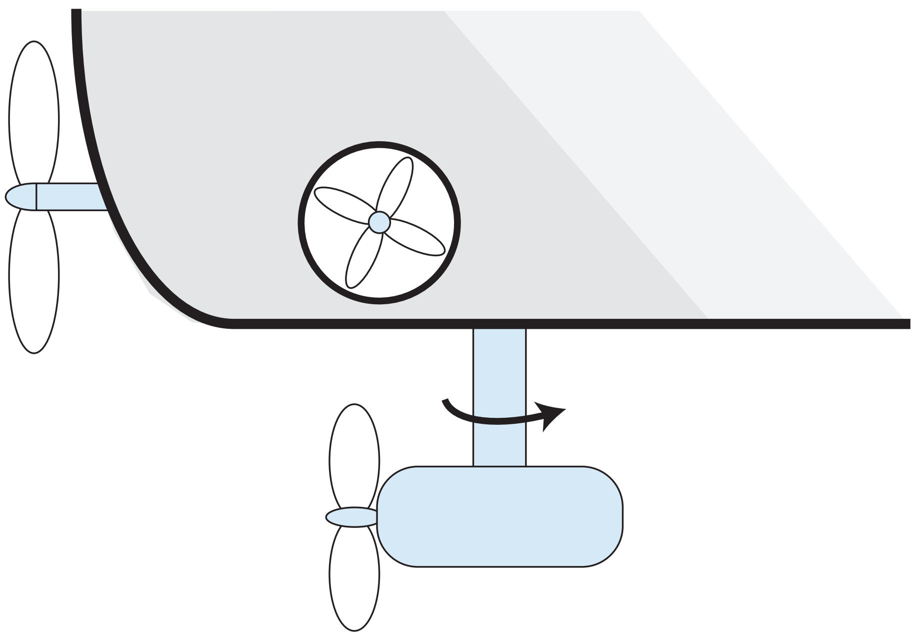

Figure 2.2: Illustration of the various thrusters mounted aboard ships.

The ship used in this project is 250+ metre long shuttle tanker fitted with a combination of the thrusters. The thruster layout is as depicted on figure 2.3. The thruster configuration is important as this will be used in the controller to compute the influence each thruster has on the vessel, for instance, the sideways thrusters are not able to alter the forward motion of the vessel.

Besides having the thruster configuration on figure 2.3 the weight of the ship is approximately 175000 metric tonnes and is port-starboard symmetric. The latter is common for ships as asymmetric ships are naturally course unstable.

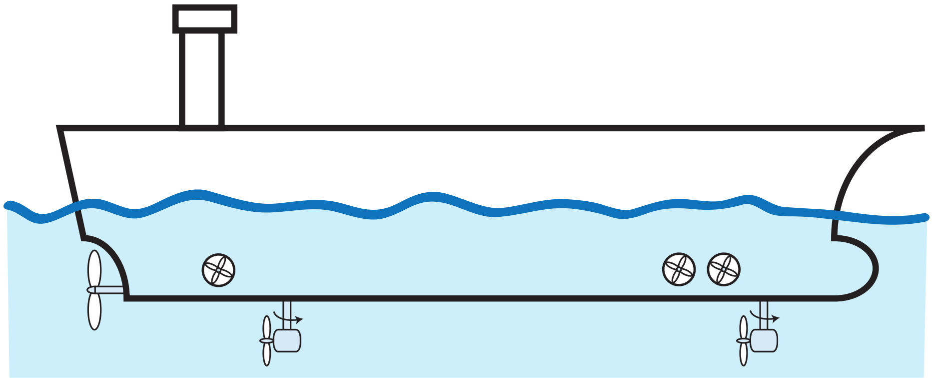

Figure 2.3: Configuration for the vessel used.

2.3 DEN-Mark 1

As described, hydrodynamic theory have been undergoing a big change over the last century, and Force Technology have developed their own tool to simulate how ships interact with fluid, named DEN-Mark1.

DEN-Mark 1 is a software simulator tool developed by Force Technology which amongst can be used to simulate how ships interact with the waters around them. The software tool is primarily used to educate crews, so they know how the vessel acts once they are to board it. The simulator is based on measured hydrodynamic coefficients of the vessel as well as the layout of the vessel, and then computes how the fluid acts on the vessel.

Several settings can be specified in the simulator software, such as current, waves and wind disturbances. The module used in this project is interfaced to Matlab to ease testing and verification.

Chapter 3
Project Scope

Throughout the introduction and analysis, the emphasis have been on improving the existing technologies. This chapter will try to create a scope for the project based on the analysis.

The requirements to a DP system is hard to specify, but generally the ship owners set some minimum bounds the vessel should stay within, to avoid wear and tear of the pipeline connecting the ship to the oil field. As written in the analysis in chapter 2, FORCE TECHNOLOGY are currently verifying if these criteria are met.

3.1 Main Scope

TTo improve on the existing system, the following criteria can be specified as; develop a non-linear model, a non-linear estimator as well as a non-linear controller. Dynamic thrust allocation could prove beneficial, as the computation of the thrust lookup-table is time consuming and if a small change is made (ex. disabling a thruster), the tables are to be computed all over again.

- Develop a non-linear model
- Develop a non-linear controller
- Develop a non-linear estimator
- *Extra:* Develop a dynamic thrust allocating module

The old system was depicted on figure 2.1 and a figure with the suggested system depicted on figure 3.1.

3.2 Verification Tests

To verify whether the suggested system works as intended and produce better results than the current configuration. The following section will describe the test set-up

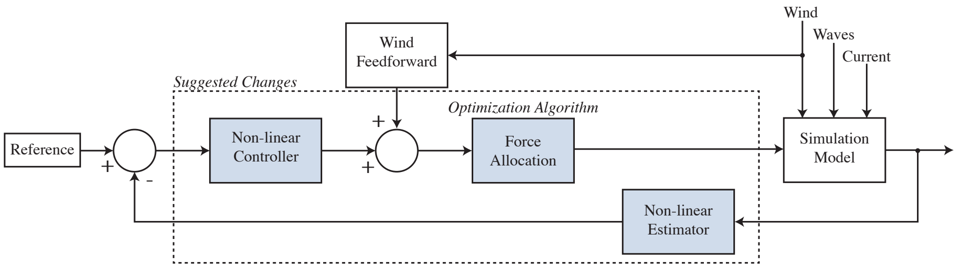

Figure 3.1: Illustration of the proposed control configuration, it should be noted that the optimization just serves as a map to the thrusters.

used to verify if and by how much the performance is improved.

To compare the two systems, a series of tests will be carried out. Currently, the tests are carried out to determine the angle at which the system cannot maintain its position when attenuated by waves, current and wind. This is done by changing the angle of attack of the vessel with respect to the disturbances. The following test specification is based on a representative scenario used at FORCE TECHNOLOGY for model testing.

This test specification includes tests from different angles of attack as well as failure scenarios (thruster failure modes). The thruster failures tests will however not be performed as vessels normally abandon the operation if their thrusters are failing. These tests will form the basis for the verification of the system. All of the tests are carried out with the following environmental conditions:

- Wind: 15 m/s
- Current: 2 knots
- Waves: JONSWAP, Hs = 5, Tp = 8.6

These tests are then performed for different angles of attack ranging from 0 to 15 degrees in steps of 5. Giving a total of 7 tests for each control system. If the derived model provides the same response as that of DEN-Mark1, this will serve as the test bed of the systems.

3.3 Measure of Performance

To qualitatively be able to say something about the performance of the system as well as compare them to the current control configuration used at FORCE TECHNOLOGY

. Some sort of performance measure must be established. As the common objective is to stay within some bound, no matter the disturbances, the first performance measure will be the maximum deviation from the origin $(0, 0, 0)$. This will serve as a reference when comparing the two systems. This deviation forms the basis for the deviation plots described in 3.3.2. The second performance measure are a performance index based on a cost function. Both the estimator and the control system will be evaluated and compared with that of the linear PID controller. The estimator performance function is described in 3.3.1 and that of the control system is described in the last part of 3.3.2.

3.3.1 Estimator Performance

The performance of the estimator will be evaluated using a simulation. The position of the vessel should be better than the one with no filter, even though the system is contaminated with noise. The plot will be an x, y-plot giving the vessels position both with and without the estimator running.

3.3.2 Controller Performance

The controller performance will be evaluated in two ways. First, a deviation plot that shows the biggest deviation with a box. The corners of this box is generated by the biggest and smallest value along the x and y axis respectively, this is shown on figure 3.2. The other performance criteria is a performance function, which is described in (3.1).

Figure 3.3 shows an example of a deviation plot, where several disturbance angles are plotted on the same figure. The performance functios are described below as in (3.1). Deviation plots will be normalized with the ship length, for the x and y axis respectively - as this will give a better impression of the performance of the controller, rather than just the deviation in metres. The overall performance of the controllers will be evaluated with the a performance measure, given as in (3.1).

$$\mathcal{J} = \sum_{k=0}^{n} \boldsymbol{x}_k^T \boldsymbol{Q} \boldsymbol{x}_k + \boldsymbol{u}_k^T \boldsymbol{R} \boldsymbol{x}_k \tag{3.1}$$

With weights $\boldsymbol{Q}$ and $\boldsymbol{R}$ being symmetric and positive definite, with entries selected using Bryson and Hos rule as defined in [GFFEN09], suggesting the following choice of weights:

$$Q_{ii} = \frac{1}{\max(x_i)^2} \tag{3.2}$$

$$R_{ii} = \frac{1}{\max(u_i)^2} \tag{3.3}$$

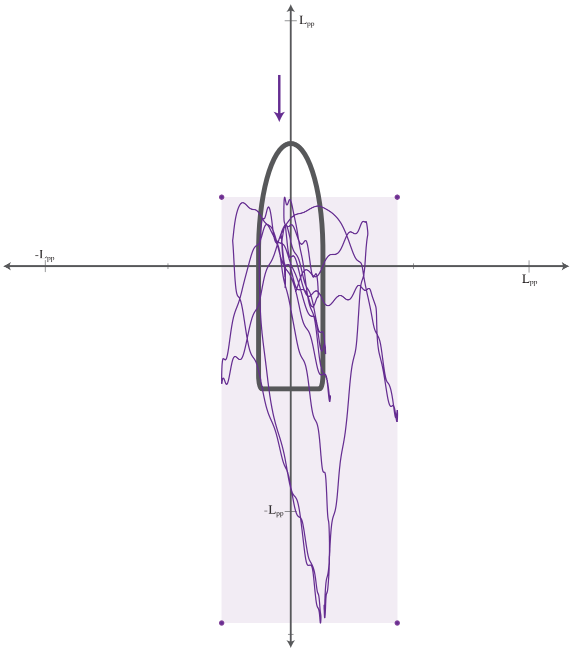

Figure 3.2: An example position of a vessel, and the deviation box on top of it. The maximum deviation points spanning the box is generated by the (x, y) coordinates of the maximum and minimum points.

This will provide a performance index of the control system, as the control signal is compared to the deviation, and everything is normalized with respect to the highest deviation. Comparison of the two systems will be done both in the deviation plot, but also the performance index.

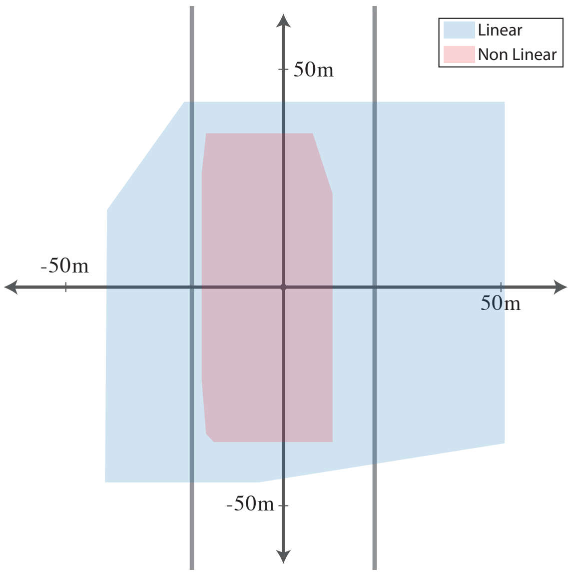

Figure 3.3: Example of a deviation plot, with the blue field being the configuration currently used at FORCE TECHNOLOGY , and the green being the proposed algorithm.

Chapter 4

Kinematics

4.1 Notation

Throughout this chapter the geometrical aspects of the vessel modelling will be described. The matrices presented in this chapter describes the rotation of a system moving inside another system. Two main systems (or reference frames) of motion are used. The body fixed frame (denoted $BODY$) and the local fixed frame (denoted NED for North-East-Down). The body frame is non-inertial, and rotates within the inertial NED-frame.

A general model of the vessel in the two frames, are by [Fos11] defined as in (4.1) and (4.2). The motion given by $\boldsymbol{\eta}$ in (4.1) is in the local frame, whereas the motion by $\boldsymbol{\nu}$ in (4.2) is in the body fixed.

$$\dot{\boldsymbol{\eta}} = \boldsymbol{J}_{\boldsymbol{\Theta}}(\boldsymbol{\eta})\boldsymbol{\nu} \tag{4.1}$$

$$\boldsymbol{M}\dot{\boldsymbol{\nu}} + \boldsymbol{C}(\boldsymbol{\nu})\boldsymbol{\nu} + \boldsymbol{D}(\boldsymbol{\nu})\boldsymbol{\nu} + \boldsymbol{g}\boldsymbol{\eta} + \boldsymbol{g}_0 = \boldsymbol{\tau} + \boldsymbol{\tau}_{wind} + \boldsymbol{\tau}_{wave} \tag{4.2}$$

With the state vectors $\boldsymbol{\eta} = [x, y, z, \phi, \theta, \psi]^T$ and $\boldsymbol{\nu} = [u, v, w, p, q, r]^T$ being desribed in 4.1. This equations states that BODY-fixed velocities $\boldsymbol{\nu}$, corresponds to NED-fixed velocities $\dot{\boldsymbol{\eta}}$, through the rotation matrix $\boldsymbol{J}_{\boldsymbol{\Theta}}(\boldsymbol{\eta})$. This chapter deals with these rotations. To maintain a uniform notation in the report, the [SNA50] notation will be used throughout. The following table 4.1 denotes the different variables used throughout the report.
As with the notation used in the different coordinate systems, the rotation matrices between the individual reference frames are noted by the following to keep track of individual matrices.

$$\boldsymbol{x}^{\text{to}} = \boldsymbol{R}^{\text{to}}_{\text{from}}\boldsymbol{x}^{\text{from}} \tag{4.3}$$

To be interpreted as moving from one reference frame to another, through the transformation matrix $\boldsymbol{R}$ with the *to* and *from* describing the frames being converted to and from, with n denoting the NED-frame, and b denoting the BODY-frame.

Description	Forces and moments	Linear and angular velocities	Position and Euler angles
motion in x direction (surge)	X	u	x
motion in y direction (sway)	Y	v	y
motion in z direction (heave)	Z	w	z
rotation about x axis (roll)	K	p	ϕ
rotation about y axis (pitch)	M	q	θ
rotation about z axis (yaw)	N	r	ψ

Table 4.1: SNAME notation for marine vessels

4.2 Reference Frames

This project mainly concerns two reference frames, the NED and BODY frame, several others exist, but are omitted due to the other two being sufficient to describe the motion. Figure 4.1 depicts how the NED and BODY frame coincide.

NED-frame:

The inertial NED-frame (North-East-Down) is a tangent plane to the earth's surface, with the x-axis aligned to the north, the y-axis aligned east, and the z-axis pointing downwards. This form of navigation is termed as flat earth navigation, and holds true when the ship does not deviate too much from the origin of the plane due to the curvature of the earth.

BODY-frame:

The BODY-frame is a non-inertial reference frame, with origin somewhere in the NED-frame. This frame will be used to describe all linear and angular velocities. The origin of the frame is denoted Centre of Origin (CO) and is chosen somewhere in the waterline of the vessel. The calculations are however easier if this point coincides with the CG.

4.3 Rotation Matrices

The rotation matrix $\boldsymbol{J}_{\boldsymbol{\Theta}}(\boldsymbol{\eta})$ in (4.1) is the only equation in the model that includes a kinematic term. This matrix describes the translation from one reference frame to another. This matrix contains two sub-matrices on the diagonal, and is by [Fos11]

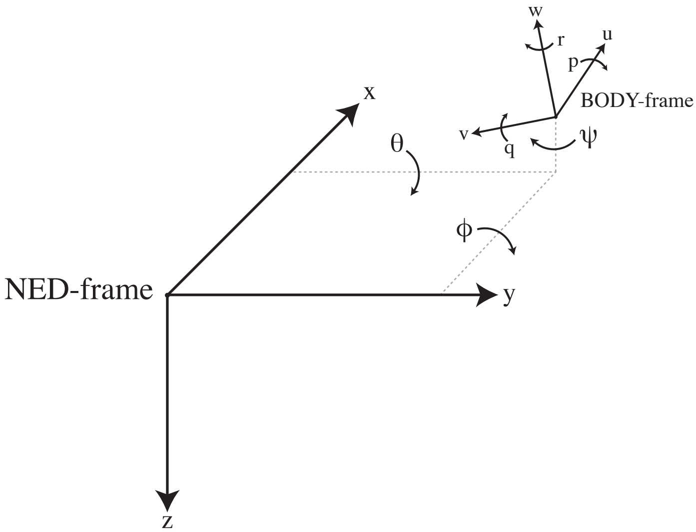

Figure 4.1: The NED and BODY-frame and their interactions depicted.

given as:

$$\boldsymbol{J}_\Theta(\boldsymbol{\eta}) = \begin{bmatrix} \boldsymbol{R}_b^n(\boldsymbol{\Theta}_{nb}) & \boldsymbol{0}_{3\times3} \\ \boldsymbol{0}_{3\times3} & \boldsymbol{T}_\Theta(\boldsymbol{\Theta}_{nb}) \end{bmatrix} \tag{4.4}$$

With $\boldsymbol{R}(\boldsymbol{\Theta})$ describing the rotation of the linear velocities, and $\boldsymbol{T}(\boldsymbol{\Theta})$ describing the rotation of the rotational velocities. The vector $\boldsymbol{\Theta}$ contains the individual angle elements $[\phi, \theta, \psi]$. The rotation matrices describing $\boldsymbol{R}(\boldsymbol{\Theta})$ are based on the Euler angle transformation which is based on 3 principle rotation matrices around the individual axes, given by (4.5) for rotation about the x, y and z axis respectively.

$$\boldsymbol{R}_{x,\phi} = \begin{bmatrix} 1 & 0 & 0 \\ 0 & c\phi & -s\phi \\ 0 & s\phi & c\phi \end{bmatrix}, \boldsymbol{R}_{y,\theta} = \begin{bmatrix} c\theta & 0 & s\theta \\ 0 & 1 & 0 \\ -s\theta & 0 & c\theta \end{bmatrix}, \boldsymbol{R}_{z,\psi} = \begin{bmatrix} c\psi & -s\psi & 0 \\ s\psi & c\psi & 0 \\ 0 & 0 & 1 \end{bmatrix} \tag{4.5}$$

$\boldsymbol{R}(\boldsymbol{\Theta})$ is given as a product of these 3 rotations. The order at which these rotations are carried out are not random, as several combinations can give the same answer. [SNA50] suggest using a zyx-rotation (rotation about the z-axis, then the y-axis and then the x-axis), which gives the rotation matrix as the following product:

$$\boldsymbol{R}_b^n(\boldsymbol{\Theta}_{nb})\boldsymbol{R}_{z,\psi}\boldsymbol{R}_{y,\theta}\boldsymbol{R}_{x,\phi} = \begin{bmatrix} c\psi c\theta & -s\psi c\phi + c\psi s\theta s\phi & s\psi s\phi + c\psi c\phi s\theta \\ s\psi c\theta & c\psi c\phi + s\phi s\theta s\psi & -c\psi s\phi + s\theta s\psi c\phi \\ -s\theta & c\theta s\phi & c\theta c\phi \end{bmatrix} \tag{4.6}$$

With $c(\cdot)$ and $s(\cdot)$ being $\cos(\cdot)$ and $\sin(\cdot)$ respectively. Rotation matrices are orthogonal of nature, which implies that when multiplied with their transpose they equal the identity matrix, thus:

$$\boldsymbol{R}(\boldsymbol{\Theta})\boldsymbol{R}(\boldsymbol{\Theta})^T = \boldsymbol{R}(\boldsymbol{\Theta})^T\boldsymbol{R}(\boldsymbol{\Theta}) = \boldsymbol{I} \tag{4.7}$$

Furthermore, the cross product operator $\boldsymbol{S}(\boldsymbol{x})$ can be used to compute the crossproduct between two vectors. The operator $\boldsymbol{S} : \mathbb{R}^3 \rightarrow \mathbb{R}^3$ is defined as in equation (4.8):

$$\boldsymbol{S}(\boldsymbol{x}) = -\boldsymbol{S}^T(\boldsymbol{x}) = \begin{bmatrix} 0 & -x_3 & x_2 \\ x_3 & 0 & -x_1 \\ -x_2 & x_1 & 0 \end{bmatrix} \tag{4.8}$$

As the rotation of linear motion is fairly straight forward, the rotation of the angular positions are a bit harder to compute. The angular rotation matrix is a bit different as the integral of the angular velocities in the body frame does not have any physical interpretation. The rotation matrix is by [Fos11] defined as:

$$\boldsymbol{T}_\Theta(\boldsymbol{\Theta}_{nb}) = \begin{bmatrix} 1 & s\phi c\theta & c\phi t\theta \\ 0 & c\phi & -s\phi \\ 0 & s\phi/c\theta & c\phi/c\theta \end{bmatrix}, \theta \neq \pm 90^\circ \tag{4.9}$$

With $t(\cdot)$ being $\tan(\cdot)$. In equation (4.9) the pitch of the ship θ should differ from $\pm 90^\circ$, or else the equation becomes infinity and the equation does not hold. This is known as a gym-ball lock, and can be countered by using unit-quaternions instead. However, a ship should never encounter pitch angles of $\pm 90^\circ$. Thus, the final rotation can be computed as:

$$\dot{\boldsymbol{\eta}} = \boldsymbol{J}_{\boldsymbol{\Theta}}(\boldsymbol{\eta})\boldsymbol{\nu} \Leftrightarrow \begin{bmatrix} \dot{\boldsymbol{p}}^n_{b/n} \\ \dot{\boldsymbol{\Theta}}_{nb} \end{bmatrix} = \begin{bmatrix} \boldsymbol{R}^n_b(\boldsymbol{\Theta}_{nb}) & \boldsymbol{0}_{3\times 3} \\ \boldsymbol{0}_{3\times 3} & \boldsymbol{T}_\Theta(\boldsymbol{\Theta}_{nb}) \end{bmatrix} \begin{bmatrix} \boldsymbol{v}^b_{b/n} \\ \boldsymbol{\omega}^b_{b/n} \end{bmatrix} \tag{4.10}$$

With $\dot{\boldsymbol{\eta}} = [\dot{\boldsymbol{p}}^n_{b/n}, \dot{\boldsymbol{\Theta}}_{nb}]^T$ being the linear and angular velocities in the NED-frame, and $\boldsymbol{\nu} = [\boldsymbol{v}^b_{b/n}, \boldsymbol{\omega}^b_{b/n}]^T$ the velocities in the BODY-frame.

4.4 Concluding Remarks

Throughout this chapter, kinematics for the model in (4.1) have been derived and described. This forms the basis for many navigation systems aboard vessels, as different sensors are measuring in different reference frames. The dynamics of the rotation matrices was also described, and a cross product operator was presented.

The following chapter will describe the kinetics of (4.2).

Chapter 5

Kinetics

The controller and estimator will be based on a model of the vessel, which should be sufficiently precise without overcomplicating the computations carried out at each iteration. For ease and to present the notation, a general vectorial model developed by [Fos11] will be used throughout. The model consists of 2 parts, a static part describing the forces that are directly linked to the mass and inertial properties of the vessel, and a hydrodynamic part describing the forces acting on the vessel due to the fluid affecting the vessel.

A general 6-DOF vessel can as in (4.1) and (4.2) be stated as:

$$\dot{\boldsymbol{\eta}} = \boldsymbol{J}_{\boldsymbol{\Theta}}(\boldsymbol{\eta})\boldsymbol{\nu} \tag{5.1}$$

$$\boldsymbol{M}\dot{\boldsymbol{\nu}} + \boldsymbol{C}(\boldsymbol{\nu})\boldsymbol{\nu} + \boldsymbol{D}(\boldsymbol{\nu})\boldsymbol{\nu} + \boldsymbol{g}(\boldsymbol{\eta}) + \boldsymbol{g}_0 = \boldsymbol{\tau}_{ctrl} + \boldsymbol{\tau}_{dist.} \tag{5.2}$$

Where the kinematics chapter described the rotation matrix equation $\boldsymbol{J}_{\boldsymbol{\Theta}}(\boldsymbol{\eta})$ were described in the previous chapter, this chapter describes the individual matrices in the kinetic model connected to (5.2) as well as the derivations hereof.

At the end of the chapter a control model will be derived from the general model in (5.1) and (5.2), as heave, roll and pitch motions are uncontrollable during station keeping operations for shuttle tankers, these are omitted. Also, as the velocity is close to zero, assumptions about the hydrodynamic derivatives according to [Fos11] and [ALdC98] can be made, using properties from the port-aft symmetry - thus further reducing the order of the model.

5.1 Mass matrix

The mass matrix consists of two main parts. One describing general equations of motion $\boldsymbol{M}_{RB}$ and one that describes added mass and hydrodynamic derivatives $\boldsymbol{M}_A$.

The static part, $\boldsymbol{M}_{RB}$ are easily determined from equation Newtons second law of motion $F_x = m\ddot{x}$ and Newtons law of rotation $\tau_x = I_x \alpha_x$, thus, when put on matrix from as in (5.2) giving the static matrix as:

$$\boldsymbol{M}_{RB} = \begin{bmatrix} m\boldsymbol{I}_{3\times 3} & \boldsymbol{0}_{3\times 3} \\ \boldsymbol{0}_{3\times 3} & \boldsymbol{I}_b \end{bmatrix} \tag{5.3}$$

Where: m is the mass of the vessel and $\boldsymbol{I}_b$ the inertial tensor matrix, with the moments of inertia about the respective axes on the diagonal.

If the centre of gravity and the centre of floatation are misaligned, the matrix $\boldsymbol{M}_{RB}$ in equation (5.3) will contain additional moments and forces on the anti-diagonal. These elements are given as the moment generated by this misalignment. The moment is equal to the cross product of the two force vectors, which can be represented by the vector cross-product operator in (4.8). To account for these forces and moments, the cross product operand in (4.8) is added on the anti-diagonal with the misalignment vector as input. This gives the final expression for the rigid-body matrix $\boldsymbol{M}_{RB}$:

$$\boldsymbol{M}_{RB} = \begin{bmatrix} m\boldsymbol{I}_{3\times 3} & -m\boldsymbol{S}(\boldsymbol{r}_g^b) \\ m\boldsymbol{S}(\boldsymbol{r}_g^b) & \boldsymbol{I}_b \end{bmatrix} \tag{5.4}$$

The hydrodynamic part of the mass matrix $\boldsymbol{M}_A$ consists mainly of added-mass elements acting on the vessel as it pushes through the water. The derivations of these elements are omitted from this thesis, as they are out of the scope of the project. The derivations of the individual elements was derived by [Lam95] but converted to matrix form in [Fos02] which gives the added-mass matrix as in (5.5):

$$\boldsymbol{M}_A = \begin{bmatrix} -X_{\dot{u}} & -X_{\dot{v}} & -X_{\dot{w}} & -X_{\dot{p}} & -X_{\dot{q}} & -X_{\dot{r}} \\ -X_{\dot{v}} & -Y_{\dot{v}} & -Y_{\dot{w}} & -Y_{\dot{p}} & -Y_{\dot{q}} & -Y_{\dot{r}} \\ -X_{\dot{w}} & -Y_{\dot{w}} & -Z_{\dot{w}} & -Z_{\dot{p}} & -Z_{\dot{q}} & -Z_{\dot{r}} \\ -X_{\dot{p}} & -Y_{\dot{p}} & -Z_{\dot{p}} & -K_{\dot{p}} & -K_{\dot{q}} & -K_{\dot{r}} \\ -X_{\dot{q}} & -Y_{\dot{q}} & -Z_{\dot{q}} & -K_{\dot{q}} & -M_{\dot{q}} & -M_{\dot{r}} \\ -X_{\dot{r}} & -Y_{\dot{r}} & -Z_{\dot{r}} & -K_{\dot{r}} & -M_{\dot{r}} & -N_{\dot{r}} \end{bmatrix} \tag{5.5}$$

This leaves the final mass matrix as the sum of (5.4) and (5.5):

$$\boldsymbol{M} = \boldsymbol{M}_{RB} + \boldsymbol{M}_A = \boldsymbol{M}^T > 0 \tag{5.6}$$

As both (5.4) and (5.5) are symmetric, the sum of the two will also be symmetric and positive definite. This corresponds to the assumption that the vessel is port-starboard symmetric.

5.2 Coriolis-Centripetal matrix

The Coriolis-Centripetal matrix represents the added forces and moments given by the vessel rotating in an inertial frame, with the Coriolis term stemming from the motion of a rotating system, and the centripetal term from the rotation of a rotating system. It is possible to find a number of ways to represent this vector. For simplicity, and keeping in line with the rest of the report, the derivation from [Fos11] will be used.

Just as with the mass matrix given in (5.6) this matrix also consist of a static part $\boldsymbol{C}_{RB}$ and a hydrodynamic part $\boldsymbol{C}_A$ - both of them are dependent on the body-fixed velocity vector $\boldsymbol{\nu}$. The sum of these two can according to [FS91] however always be parametrized from the mass matrix in (5.6) such that $\boldsymbol{C}(\boldsymbol{\nu}) = -\boldsymbol{C}^T(\boldsymbol{\nu})$ as:

$$\boldsymbol{C}(\boldsymbol{\nu}) = \begin{bmatrix} \mathbf{0}_{3\times3} & -\boldsymbol{S}(\boldsymbol{M}_{11}\boldsymbol{\nu}_1 + \boldsymbol{M}_{12}\boldsymbol{\nu}_2) \\ -\boldsymbol{S}(\boldsymbol{M}_{11}\boldsymbol{\nu}_1 + \boldsymbol{M}_{12}\boldsymbol{\nu}_2) & -\boldsymbol{S}(\boldsymbol{M}_{21}\boldsymbol{\nu}_1 + \boldsymbol{M}_{22}\boldsymbol{\nu}_2) \end{bmatrix} \tag{5.7}$$

With $\boldsymbol{S}$ being the cross-product operand defined in (4.8) and the submatrices $\boldsymbol{M}_{ii}$ stemming from (5.6) as:

$$\boldsymbol{M} = \begin{bmatrix} \boldsymbol{M}_{11} & \boldsymbol{M}_{12} \\ \boldsymbol{M}_{21} & \boldsymbol{M}_{22} \end{bmatrix} \tag{5.8}$$

With the velocity vectors $\boldsymbol{\nu}_i$ defined as the first 3 and last 3 components of $\boldsymbol{\nu}$ respectively $\boldsymbol{\nu}_1 = [u, v, w]^T$ and $\boldsymbol{\nu}_2 = [p, q, r]^T$ respectively.

5.3 Damping

The damping forces are divided into two terms. One describing the non-linear parts, and one describing the linear. The linear damping terms are determined from model tests. The non-linear terms are however much harder to compute, as these depend on several hydrodynamic parameters and phenomena that are hard to determine accurately. For station keeping operations, the non-linear terms are relatively small, and the linear damping terms will dominate as illustrated on figure 5.1.

The damping part is as the mass matrix $\boldsymbol{M}$ and the coriolis-centripetal matrix $\boldsymbol{C}$ also defined by two parts a constant (linear) and a dynamic part (non-linear). Generally, these two are defined as:

$$\boldsymbol{D}(\boldsymbol{\nu}) = \boldsymbol{D}_L\boldsymbol{\nu} + \boldsymbol{d}_{NL}(\boldsymbol{\nu}) \tag{5.9}$$

With $\boldsymbol{D}$ being the linear coefficients defined as in (5.10) and $\boldsymbol{d}_{NL}$ the non-linear counterpart defined as in (5.11). However, the cross damping coefficients are hard to

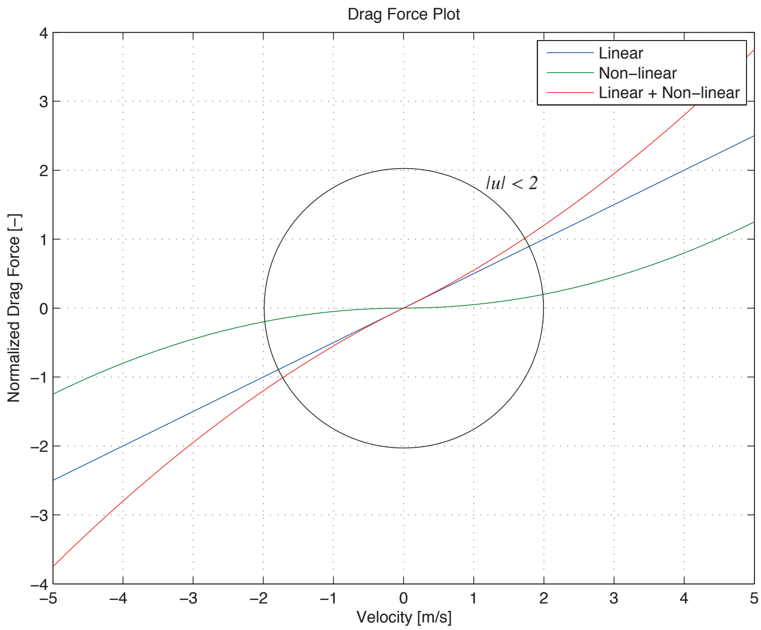

Figure 5.1: Plot of the drag forces around zero speed. As seen the linear part will dominate the non-linear one at low speeds, so for station keeping purposes, the linear damping matrix will add the largest contribution to the damping force.

define for the roll, pitch and heave motion, so generally these are only defined for 3 degrees of freedom, therefore the following matrices are only defined for 3 degrees of freedom as:

$$\boldsymbol{D}_L = \begin{bmatrix} -X_u & 0 & 0 \\ 0 & -Y_v & -Y_r \\ 0 & -N_v & -N_r \end{bmatrix} \tag{5.10}$$

$$\boldsymbol{d}_{NL}(\boldsymbol{\nu}) = \begin{bmatrix} -X_{|u|u}|u| & 0 & 0 \\ 0 & -Y_{|v|v}|v| & -Y_{|v|r}|v| \\ 0 & -N_{|v|v}|v| & -N_{|v|r}|v| \end{bmatrix} \tag{5.11}$$

These two matrices (5.10) and (5.11) are only for 3 degrees of freedom, but as will be described later, this will be sufficient for dynamic positioning operations.

5.4 Restoring forces

The restoring forces, describes a vessels ability to return to its equilibrium after being affecting in either pitch, roll or heave. This stability parameter can be defined by the metacentre of the vessel, which is described by a line running through the Centre of Buoyancy (CB), and then see how this changes once the vessel is moved away from its equilibrium, this can be seen on figure 5.2.

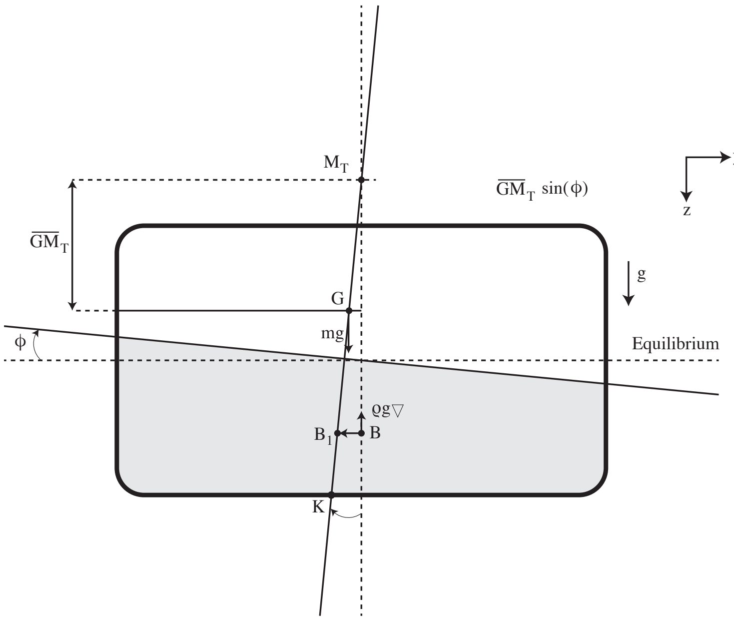

Figure 5.2: Definition of metacentre of a tilted vessel.

From Archimedes and Newton, it is known that a vessel at rest will be acted upon by no forces or two forces of equal magnitude, for submerged vessels this means that the force generated down by the mass of the ship, is cancelled out by a force of equal magnitude in the opposite direction. This makes way for the definition in , stating that the mass m multiplied with the gravitational acceleration g is equal to the density of the water ρ multiplied with the gravitational acceleration g and the fluid displaced ∇.

$$mg = \rho g \nabla \tag{5.12}$$

If z is defined as the position in heave (with z positive downwards, and $z = 0$ being the vessels equilibrium), the force acting on the vessel can be defined as a function of a change in displacement, thus rewriting the Archimedian principle given in equation

(5.12) as:

$$Z = mg - \rho g[\nabla + \delta\nabla(z)] \tag{5.13}$$
$$= -\rho g \delta\nabla(z) \tag{5.14}$$

Where $\nabla(z)$ is a function of the change in displacement of the vessel when deviating from the equilibrium (either resulting in a positive force downwards of a negative force upwards pushing the vessel towards the equilibrium). According to [Fos11] this force can be written as:

$$\delta\nabla(z) = \int_0^z A_{wp}(\zeta)d\zeta \tag{5.15}$$

With $A_{wp}(\zeta)$ being a function of how the water plane area changes depending on the height of the vessel. However, for small perturbations around the equilibrium $\delta\nabla z$, the water plane are of the ship can be assumed constant, so $A_{wp}(\zeta) \approx A_{wp}(0)$. Which collapses equation (5.14) to equation (5.16):

$$Z = -\rho g A_{wp}(0)z \tag{5.16}$$

As these forces are acting on the body in the NED frame, they have to be translated to the BODY-frame, by the inverse rotation matrix, thus:

$$\delta \boldsymbol{f}_r^b = \boldsymbol{R}_b^n(\boldsymbol{\Theta_{nb}})^{-1}\delta\boldsymbol{f}_r^n \tag{5.17}$$
$$= \boldsymbol{R}_b^n(\boldsymbol{\Theta_{nb}})^{-1}\begin{bmatrix} 0 \\ 0 \\ -\rho g \int_0^z A_{wp}(\zeta)d\zeta \end{bmatrix} \tag{5.18}$$

Which when computed, gives an expression for the restoring force in the body frame $\delta\boldsymbol{f}^b$ as:

$$\delta\boldsymbol{f}^b = -\rho g \begin{bmatrix} -\sin(\theta) \\ \cos(\theta)\sin(\phi) \\ \cos(\theta)\cos(\phi) \end{bmatrix} \int_0^z A_{wp}(\zeta)d\zeta \tag{5.19}$$

This computes the forces acting on the ship along the axes, however, the moments generated will be a function of the metacentric arms (the deviation from the equilibrium), this vector can be given for roll and pitch as:

$$\boldsymbol{r}_r^b = \begin{bmatrix} -\overline{GM}_L sin(\theta) \\ \overline{GM}_T \sin(\phi) \\ 0 \end{bmatrix} \tag{5.20}$$

With the force given as the buoyancy (or the downwards force) acting along the z-axis of the vessel. Thus defining the force $\boldsymbol{f}_r^b$ in the body frame as:

$$\boldsymbol{f}_r^b = \boldsymbol{R}_b^n(\boldsymbol{\Theta}_{nb})^{-1} \begin{bmatrix} 0 \\ 0 \\ -\rho g \nabla \end{bmatrix} = -\rho g \nabla \begin{bmatrix} -\sin(\theta) \\ \cos(\theta)\sin(\phi) \\ cos(\theta)\cos(\phi) \end{bmatrix} \tag{5.21}$$

Finally defining the restoring moments as the crossproduct between the force and the distance between them, using the the cross-product operator defined in equation (4.8) the moments are obtained as in equation (5.23):

$$\boldsymbol{m}_r^b = \boldsymbol{r}_r^b \times \boldsymbol{f}_r^b \tag{5.22}$$

$$= -\rho g \nabla \begin{bmatrix} \overline{GM}_T \sin(\phi)\cos(\theta)\cos(\phi) \\ \overline{GM}_L \sin(\theta)\cos(\theta)\cos(\phi) \\ (-\overline{GM}_L \cos(\theta) + G\bar{M}_T)\sin(\phi)\sin(\theta) \end{bmatrix} \tag{5.23}$$

Which then makes it possible to define the final restoring force vector $\boldsymbol{g}(\boldsymbol{\eta})$ as:

$$\boldsymbol{g}(\boldsymbol{\eta}) = \begin{bmatrix} \delta \boldsymbol{f}^b \\ \boldsymbol{m}_r^b \end{bmatrix} \tag{5.24}$$

5.5 Control and Estimator Model

To establish a model for the controller and the estimator, several assumptions can be made, with the goal to reduce the model and thereby the complexity of the system as a whole. Mainly, in station keeping operations the velocity of the vessel is (or close to) zero, which negates all velocity dependent constants from the system defined in (5.1) and (5.2).

The works of [YB98] have shown that the roll motion of a ship can be damped by using the rudder, this does however require a forward velocity, so trying the control the roll motion with zero forward velocity is impossible. The heave motion of the vessel is also uncontrollable as well as the pitch motion. This reduces the original 6-DOF system to a 3-DOF system, with the new state space being defined as in (5.25):

$$\boldsymbol{\eta} = \begin{bmatrix} x \\ y \\ \psi \end{bmatrix}, \quad \boldsymbol{\nu} = \begin{bmatrix} u \\ v \\ r \end{bmatrix} \tag{5.25}$$

The assumption that the velocity of the vessel is close to zero, allows for the system to be redefined into two parts as in [Fos11]; one containing the static hydrodynamics of the vessel and one describing the dynamic hydrodynamics. On matrix form, they look like the following, given in (5.26) and (5.27) for the NED- and $BODY$-frame respectively:

$$\dot{\boldsymbol{\eta}} = \boldsymbol{R}(\psi)\boldsymbol{\nu} \tag{5.26}$$

$$\boldsymbol{M}\boldsymbol{\nu} + \boldsymbol{C}_{RB}(\boldsymbol{\nu})\boldsymbol{\nu} + \boldsymbol{N}(\boldsymbol{\nu}_r)\boldsymbol{\nu}_r = \boldsymbol{\tau} + \boldsymbol{\tau}_{wind} + \boldsymbol{\tau}_{wave} \tag{5.27}$$

With $\boldsymbol{N}(\boldsymbol{\nu}_r)\boldsymbol{\nu}_r$ being the dynamic hydrodynamics as a function of the relative velocity $\boldsymbol{\nu}_r$ of the vessel to the current, as in (5.28):

$$\boldsymbol{N}(\boldsymbol{\nu}_r)\boldsymbol{\nu}_r := \boldsymbol{C}_A(\boldsymbol{\nu}_r)\boldsymbol{\nu}_r + \boldsymbol{D}(\boldsymbol{\nu}_r)\boldsymbol{\nu}_r \tag{5.28}$$

The static matrices $\boldsymbol{M}$ and $\boldsymbol{C}_{RB}$ can be reduced to (5.29) and (5.30) according to [Fos02] for station keeping models in 3 degrees of freedom:

$$\boldsymbol{M} = \begin{bmatrix} m - X_{dotu} & 0 & 0 \\ 0 & m - Y_{\dot{v}} & mx_g - Y_{\dot{r}} \\ 0 & mx_g - Y_{\dot{r}} & I_z - N_{\dot{r}} \end{bmatrix} \tag{5.29}$$

$$\boldsymbol{C}_{RB} = \begin{bmatrix} 0 & 0 & -m(x_g r + v) \\ 0 & 0 & mu \\ m(x_g r + v) & -mu & 0 \end{bmatrix} \tag{5.30}$$

As the non-linear term of the damping matrices are hard to determine accurately for station keeping operations, [ALdC98] suggests a method to estimate these non-linear damping coefficients using a term called *current coefficients*. These stem from the current acting on the vessel at zero speed, and thus becomes the "relative speed" of the craft. For station keeping operations, this holds well, as the velocity (and thereby also the acceleration) of the vessel itself, $\boldsymbol{\nu}$, is close to zero, and the main disturbance on the vessel will thus be the current forces. These forces can according to [ALdC98] be defined as:

$$X_{current} = \frac{1}{2}\rho A_{Fc} C_X(\gamma_c) V_{rc}^2 \tag{5.31}$$

$$Y_{current} = \frac{1}{2}\rho A_{Lc} C_Y(\gamma_c) V_{rc}^2 \tag{5.32}$$

$$Y_{current} = \frac{1}{2}\rho A_{Lc} L_{oa} C_N(\gamma_c) V_{rc}^2 \tag{5.33}$$

Which then gives a force component in each direction. These are dependent on the relative velocity of the current V_{rc} and the current coefficients $C_X(\gamma_c)$. A_{Fc} is the frontal projected area, A_{Lc} is the lateral projected area and L_{oa} is the overall length of the vessel. The current velocity components are determined by the absolute velocity relative to the current V_{rc} and the angle of the current β_c, relative to the heading of the vessel ψ:

$$V_{rc} = \sqrt{(u - u_c)^2 + (v - v_c)^2} \tag{5.34}$$
$$\gamma_{rc} = -\text{atan2}((u - u_c), (v - v_c)) \tag{5.35}$$

With u_c being the velocity of the current along the x-axis. However, for station keeping operations (when $u = v = 0$), the relative current velocity $V_{rc} = V_c$ and the angle of attack can be computed as $\gamma_c = \psi - \beta_c - \pi$. The current coefficients $C_X(\gamma_c)$, $C_Y(\gamma_c)$ and $C_N(\gamma_c)$, can be approximated by the vessels Reynolds number and the relative angle of attack γ_c using trigonometric functions. [ALdC98] suggests the approximation in (5.36)-(5.40) for the x,y and ψ axis respectively.

$$C_{1C}(\gamma_c) \approx \left(\frac{0.09375}{(\log_{10}(R_e - 2)^2)} \frac{S}{TL} \right) \cos(\gamma_c) \tag{5.36}$$
$$+ \frac{1}{8} \frac{\pi T}{L} (\cos(3\gamma_c) - \cos(\gamma_c)) \tag{5.37}$$
$$C_{2C}(\gamma_c) \approx (C_Y - \frac{\pi T}{2L}) \sin(\gamma_c)|\sin(\gamma_c)| + \frac{\pi T}{2L} \sin^3(\gamma_c) \tag{5.38}$$
$$+ \frac{\pi T}{L}(1 + 0.4 \frac{C_B B}{T}) + \frac{\pi T}{L} \sin(\gamma_c)|\cos(\gamma_c)| \tag{5.39}$$
$$C_{6C}(\gamma_c) \approx -\frac{l}{L} \left(C_Y - \frac{\pi T}{2L} \right) \sin(\gamma_c)|\sin(\gamma_c)| - \frac{\pi T}{L} \sin(\gamma_c)\cos(\gamma_c)$$
$$- \left(\frac{1 + |\cos(\gamma_c)|}{2} \right)^2 \frac{\pi T}{L} \left(\frac{1}{2} - 2.4 \frac{T}{L} \right) \sin(\gamma_c)|\cos(\gamma_c)| \tag{5.40}$$

With constants defined as in the following list:

- L is the length of the vessel.
- T is the draft of the vessel.
- B is the beam of the vessel.
- C_B is the block coefficient.
- S is the wetted surface.
- R_e is the Reynolds number.
- C_Y is the lateral force coefficient.

With these forces lumped together, [Fos11] then suggests using the following non-linear control model:

$$\dot{\boldsymbol{\eta}} = \boldsymbol{R}(\psi)\boldsymbol{\nu} \tag{5.41}$$
$$\boldsymbol{M}\dot{\boldsymbol{\nu}} + \boldsymbol{C}_{RB}(\boldsymbol{\nu})\boldsymbol{\nu} + \boldsymbol{D}\exp(-\alpha V_{rc})\boldsymbol{\nu}_r + \boldsymbol{d}(V_{rc}, \gamma_{rc}) = \boldsymbol{\tau} + \boldsymbol{\tau}_{wind} + \boldsymbol{\tau}_{wave} \tag{5.42}$$

With the linear damping matrix $\boldsymbol{D}$ given as:

$$\boldsymbol{D} = \begin{bmatrix} -X_u & 0 & 0 \\ 0 & -Y_v & -Y_r \\ 0 & -N_v & -N_r \end{bmatrix} \tag{5.43}$$

The α in (5.42) is a tuning parameter to ensure convergence in station keeping operations. If the vessel is manoeuvring the non-linear damping term will dominate the linear, and this term becomes superfluous. The non-linear damping term $\boldsymbol{d}(V_{rc}, \gamma_{rc})$ defined as a function of the previously derived current coefficients:

$$\boldsymbol{d}(V_{rc}, \gamma_{rc}) = \begin{bmatrix} \frac{1}{2}\rho A_{Fc} C_X(\gamma_{rc}) V_{rc}^2 \\ \frac{1}{2}\rho A_{Lc} C_Y(\gamma_c) V_{rc}^2 \\ \frac{1}{2}\rho A_{Lc} L_{oa} C_N(\gamma_c) V_{rc}^2 - N_{|r|r}|r|r \end{bmatrix} \tag{5.44}$$

The last term in the r force is a stabilizer for the Munk moment which generates a destabilizing effect when the current moves around the vessel. This is added as the current coefficients does not include non-linear damping about the z-axis.

This sums up the modelling chapter, and a model, sufficient for the controller and estimator have been developed.

Chapter 6
Estimation

As the current test set-up at FORCE TECHNOLOGY , does not filter the measurements of the vessel but feeds these back to the control system directly - an estimator is developed to improve on these measurements, as well as provide filtering by exploiting the already well known model of the vessel. For station-keeping operations, the only two desired measurements are the position of the craft (x, y) as well as the heading ψ as these are to be kept constant throughout the operation. The non-linear passive observer, proposed by [Fos02] utilizes the already developed model of the vessel, which eases tuning - and therefore complies with the "requirement" that the overall system should be easy to tune.

6.1 Estimator Model

The model for the estimator will be based on the one developed for the controller in section 5.5. However, instead of trying to determine the current coefficients, as well as the non-linear dynamics given by the damping $\boldsymbol{d}(V_{rc}, \gamma_{rc})$ (which around zero is small compared to the linear damping) this as well as any other un-modelled dynamics can be lumped together in a bias term $\boldsymbol{b}$, which will have no physical interpretation as it is a collection of forces not accounted for in the model of the vessel. This replaces the damping term as:

$$\boldsymbol{D}(-\alpha V_{rc})\boldsymbol{\nu}_r + \boldsymbol{d}(V_{rc}, \gamma_{rc}) \approx \boldsymbol{D}\boldsymbol{\nu} + \boldsymbol{R}^T(\psi)\boldsymbol{b} \tag{6.1}$$

Where the bias term $\boldsymbol{b}$ can be described as a first order Markov model:

$$\dot{\boldsymbol{b}} = -\boldsymbol{T}^{-1}\boldsymbol{b} + \boldsymbol{w} \tag{6.2}$$

With $\boldsymbol{w}$ being a zero-mean Gaussian noise process driving the system, and $\boldsymbol{T}$ a matrix of time constants determined from the eigenvalues of the vessel, these can be found in appendix B. A noiseless model of the vessel can then be developed as:

$$\dot{\boldsymbol{\eta}} = \boldsymbol{R}(\psi)\boldsymbol{\nu} \tag{6.3}$$

$$\dot{\boldsymbol{b}} = -\boldsymbol{T}^{-1}\boldsymbol{b} \tag{6.4}$$

$$\boldsymbol{M}\dot{\boldsymbol{\nu}} = -\boldsymbol{D}(\boldsymbol{\nu}) + \boldsymbol{R}^T(\psi)\boldsymbol{b} + \boldsymbol{\tau} + \boldsymbol{\tau}_{\text{wind}} \tag{6.5}$$

$$\boldsymbol{y} = \boldsymbol{\eta} \tag{6.6}$$

However, as the bias term accounts for un-modelled dynamics (possibly also wind and currents), it does not account for the wave drift of the vessel which will move the vessel about. This needs to be accounted for by a model of the waves, which will influence the position of the vessel, thus altering the model to:

$$\boldsymbol{y} = \boldsymbol{\eta} + \boldsymbol{C}_w\boldsymbol{\xi} \tag{6.7}$$

$$\dot{\boldsymbol{\xi}} = \boldsymbol{A}_w\boldsymbol{\xi} + \boldsymbol{w} \tag{6.8}$$

With $\boldsymbol{A}_w$ being a system matrix describing the first and second order wave motions of the vessel and $\boldsymbol{C}_w$ being the output matrix, only giving the first-order motions as the second order motions are undesirable to use as a control signal, and are thus filtered out. $\boldsymbol{w}$ is a noise term driving the wave model. The development of the wave model is described in 6.1.1.

To exactly copy the dynamics of the vessel, a feedback term is introduced for each model parameter, with gains selected accordingly. The feedback term $\tilde{\boldsymbol{y}} = \boldsymbol{y} - \hat{\boldsymbol{y}}$ is the difference between the measured signal $\boldsymbol{y}$ and the estimate $\hat{\boldsymbol{y}}$. The model for the observer then becomes:

$$\dot{\hat{\boldsymbol{\xi}}} = \boldsymbol{A}_w\hat{\boldsymbol{\xi}} + \boldsymbol{K}_1(\boldsymbol{\omega})\tilde{\boldsymbol{y}} \tag{6.9}$$

$$\dot{\hat{\boldsymbol{\eta}}} = \boldsymbol{R}(\psi)\hat{\boldsymbol{\nu}} + \boldsymbol{K}_2\tilde{\boldsymbol{y}} \tag{6.10}$$

$$\dot{\hat{\mathrm{b}}} = -\boldsymbol{T}^{-1}\hat{\mathrm{b}} + \boldsymbol{K}_3\tilde{\boldsymbol{y}} \tag{6.11}$$

$$\boldsymbol{M}\dot{\hat{\boldsymbol{\nu}}} = -\boldsymbol{D}(\hat{\boldsymbol{\nu}}) + \boldsymbol{R}^T(\psi)\hat{\mathrm{b}} + \boldsymbol{\tau} + \boldsymbol{R}^T(\psi)\boldsymbol{K}_4\tilde{\boldsymbol{y}} \tag{6.12}$$

$$\hat{\mathrm{y}} = \hat{\boldsymbol{\eta}} + \boldsymbol{C}_w\hat{\boldsymbol{\xi}} \tag{6.13}$$

The structure of (6.9)-(6.12) is depicted on 6.1. The noise terms from the original terms are changed with the error signal $\tilde{\boldsymbol{y}}$, assuming that the noise of the GPS and compass are Gaussian zero mean.

6.1.1 Wave Model

As the waves will influence the position vessel, these are added to the estimator to provide a more accurate position and attitude estimate. Generally, waves contain

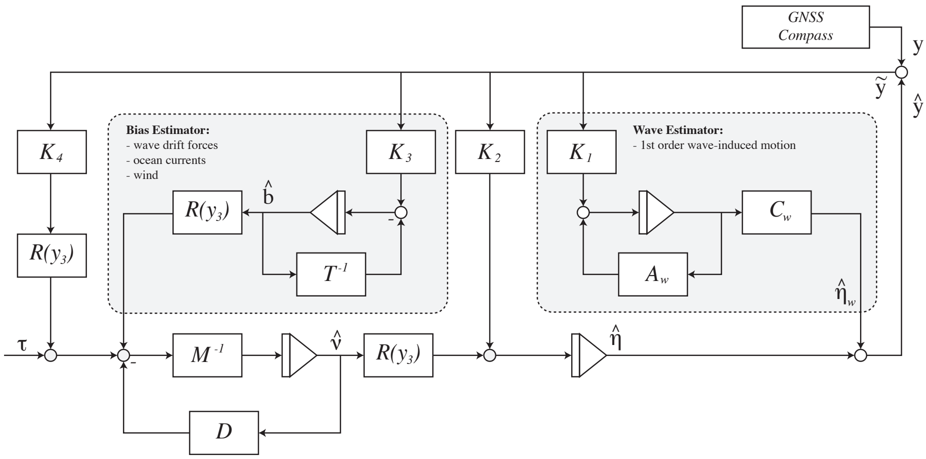

Figure 6.1: Structure of the Passive Observer.

two modes of motion, first and second order.

$$\boldsymbol{w}_{wave} = \boldsymbol{w}_1 + \boldsymbol{w}_2 \tag{6.14}$$

Where the first order motion $\boldsymbol{w}_1$ are the wave drift and the second order $\boldsymbol{w}_2$ is oscillatory motion of the vessel. The first order motions are dealt with by the controller, and can thus be seen as a disturbance. The second order motion should be filtered out, as little energy is present in these waves, but rather moves the ship back and forth in an oscillatory manner. These two orders are by [SNA50] termed low-frequency motion and wave-frequency motion for first and second order respectively. The wave motions are depicted with an example on figure 6.2.

The purpose of the wave model, is to develop a wave filter that filters out the second order motions, as these are undesirable to feed to the controller. Wave theory is worth a whole study in itself, but as the main purpose is to determine the encounter frequency - a linearised version of the wave model is sufficient. This allows to use the works of [SJ83] and [BJMS80]. More on non-linear wave theory and motion can be found in [Fos02]. The linear wave response can be computed as a second order transfer function given by:

$$h(s) = \frac{K_w s}{s^2 + 2\lambda\omega_0 s + \omega_0^2} \tag{6.15}$$

With the gains K_w and λ the only two constants to be determined. The damping term λ can be computed by fitting a non-linear least squares polynomial to the power spectrum of (6.15). However, in [Fos02] the damping is computed for a range of

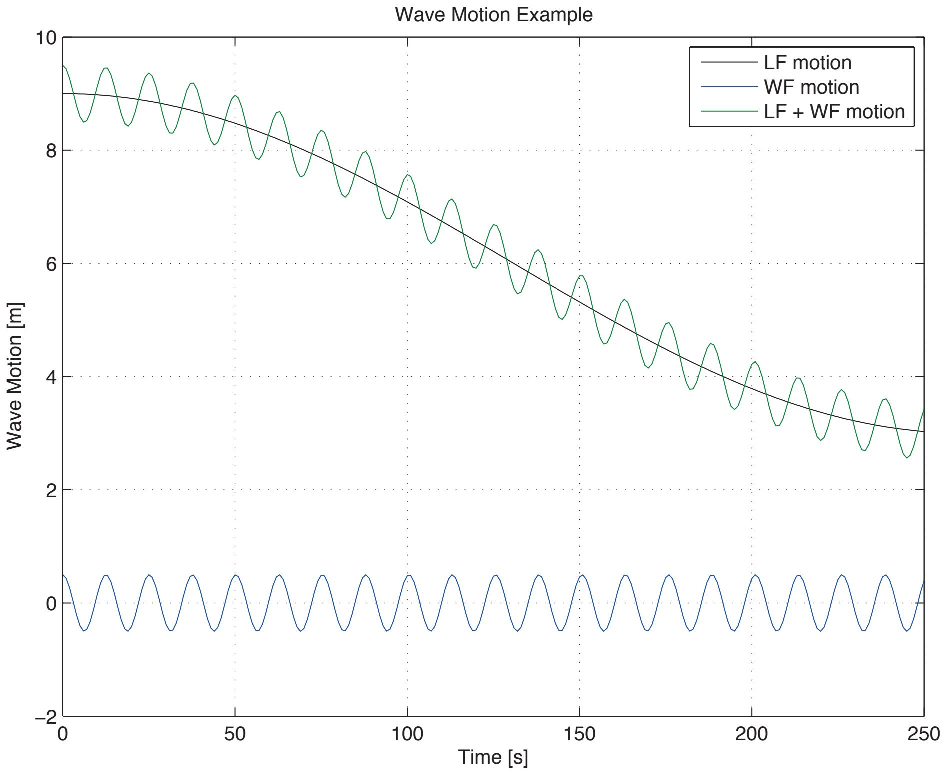

Figure 6.2: Example of the wave motion, the black line represents the first order drift countered by the controller, whereas the blue is the second order oscillatory motion.

wave periods, and all of them ≈ 0.1 for wave periods ranging from 4.4880s – 12.5664s. The gain parameter K_w can be computed as:

$$K_w = 2\lambda\omega_0\sigma \tag{6.16}$$

With σ being a parameter of the wave intensity. This parameter is dependent on the wave spectrum being used. The approximation of the wave spectra, assumes that the noise process driving the system has a unity gain over th frequency range. This allows for the intensity parameter to be equal to the highest value of the spectrum of the waves, if the approximation of the power spectrum follows the wave spectrum perfectly, the following approximation holds:

$$\sigma^2 = \max_{0<\omega<\infty} S(\omega) \tag{6.17}$$

Thus, for the test frequency specified in the tests $T_p = 8.4s$ the sigma value for the JONSWAP spectrum can be computed to be:

$$\sigma^2 = \sqrt{\max_{0<\omega<\infty} S(\omega)} = 2.2010 \tag{6.18}$$

From these definitions, it is possible to define a state space model of the wave spectra:

$$\dot{\boldsymbol{x}}_w = \boldsymbol{A}_w \boldsymbol{x}_w + \boldsymbol{e}_w w_w \tag{6.19}$$

$$y_w = \boldsymbol{c}_w^T \boldsymbol{x}_w \tag{6.20}$$

With the state vector $\boldsymbol{x}_w = [x_{w1}, x_{w2}]^T$ being the first and second order motion respectively, w_w being a Gaussian white noise process and the system matrices defined as:

$$\boldsymbol{A}_w = \begin{bmatrix} 0 & 1 \\ -\omega_0^2 & -2\lambda\omega_0 \end{bmatrix}, \quad \boldsymbol{e}_w = \begin{bmatrix} 0 \\ K_w \end{bmatrix} \tag{6.21}$$

The output matrix $\boldsymbol{c}^T = [0,\ 1]$ outputs only the second order wave motions (the oscillatory WF motion), which are then to be filtered out by the estimator. A bode plot of the frequency to be filtered out ω_0 is depicted on 6.3 This is done by a combination of a notch filter and a low pass filter, the transfer function of these are presented in

$$h_f(s) = \frac{s^2 + 2\lambda\omega_0 + \omega_0^2}{(s^2 + 2\zeta\omega_0 + \omega_0^2)(s + \omega_c)} \tag{6.22}$$

Where ω_c is the frequency at which the low-pass filter should cut off and ζ determines the notch. The parameters can be tuned to allow for small variations in the wave frequency. The tuning of (6.22) will be carried out as part of the stability analysis in 6.1.2.

6.1.2 Stability

The following error variables are defined $\tilde{\boldsymbol{\nu}} = \boldsymbol{\nu} - \hat{\boldsymbol{\nu}}$, $\tilde{\boldsymbol{\eta}} = \boldsymbol{\eta} - \hat{\boldsymbol{\eta}}$ and $\tilde{\boldsymbol{b}} = \boldsymbol{b} - \hat{\mathbf{b}}$, subtracting (6.9)–(6.12) from (6.3)–(6.5) and (6.8) respectively, the following error dynamics can be written:

$$\dot{\tilde{\boldsymbol{\xi}}} = \boldsymbol{A}_w \tilde{\boldsymbol{\xi}} - \boldsymbol{K}_1(\boldsymbol{\omega})\tilde{\boldsymbol{y}} \tag{6.23}$$

$$\dot{\tilde{\boldsymbol{\eta}}} = \boldsymbol{R}(\psi)\tilde{\boldsymbol{\nu}} - \boldsymbol{K}_2\tilde{\boldsymbol{y}} \tag{6.24}$$

$$\dot{\tilde{\boldsymbol{b}}} = -\boldsymbol{T}^{-1}\tilde{\boldsymbol{b}} - \boldsymbol{K}_3\tilde{\boldsymbol{y}} \tag{6.25}$$

$$\boldsymbol{M}\dot{\tilde{\boldsymbol{\nu}}} = -\boldsymbol{D}(\tilde{\boldsymbol{\nu}}) + \boldsymbol{R}^T(\psi)\tilde{\boldsymbol{b}} - \boldsymbol{R}^T(\psi)\boldsymbol{K}_4\tilde{\boldsymbol{y}} \tag{6.26}$$

$$\hat{\mathbf{y}} = \hat{\boldsymbol{\eta}} + \boldsymbol{C}_w\hat{\boldsymbol{\xi}} \tag{6.27}$$

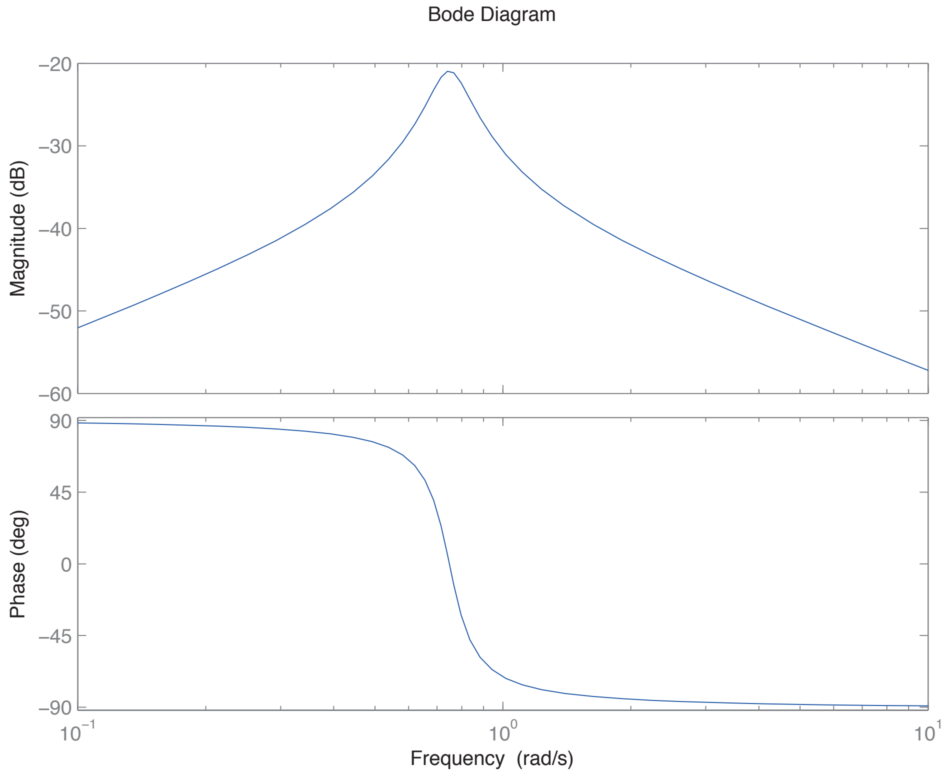

Figure 6.3: Bode diagram of the wave response of (6.15). The lobe represents the second order wave motion.

Collecting the wave model in (6.23), the bias model in (6.25) and the position model in (6.24) by defining the state vector $\tilde{\boldsymbol{x}} = [\tilde{\boldsymbol{\xi}}^T, \tilde{\boldsymbol{\eta}}^T, \tilde{\boldsymbol{b}}^T]^T$ the following state space representation of the vessels position can be established:

$$\dot{\tilde{\boldsymbol{x}}} = \boldsymbol{A}\tilde{\boldsymbol{x}} + \boldsymbol{B}\boldsymbol{R}(\psi)\tilde{\boldsymbol{\nu}} \tag{6.28}$$

$$\tilde{\boldsymbol{z}} = \boldsymbol{C}\tilde{\boldsymbol{x}} \tag{6.29}$$

With the system matrices $\boldsymbol{A}, \boldsymbol{B}$ and $\boldsymbol{C}$ defined as:

$$\boldsymbol{A} = \begin{bmatrix} \boldsymbol{A}_0 - \boldsymbol{K}_0(\boldsymbol{\omega})\boldsymbol{C}_0 & \boldsymbol{0}_{9\times 3} \\ -\boldsymbol{K}_3\boldsymbol{C}_0 & -\boldsymbol{T}^{-1} \end{bmatrix} \tag{6.30}$$

$$\boldsymbol{B} = \begin{bmatrix} \boldsymbol{B}_0 \\ \boldsymbol{0}_{3\times 3} \end{bmatrix}, \quad \boldsymbol{C} = \begin{bmatrix} \boldsymbol{K}_4\boldsymbol{C}_0 & -\boldsymbol{I}_{3\times 3} \end{bmatrix} \tag{6.31}$$

With sub-matrices defined as a sub-system excluding the bias $\boldsymbol{b}$ from the model:

$$\boldsymbol{A}_0 = \begin{bmatrix} \boldsymbol{A}_w & \boldsymbol{0}_{6\times 3} \\ \boldsymbol{0}_{3\times 6} & \boldsymbol{0}_{3\times 3} \end{bmatrix} \tag{6.32}$$

$$\boldsymbol{B} = \begin{bmatrix} \boldsymbol{0}_{6\times 3} \\ \boldsymbol{I}_{3\times 3} \end{bmatrix}, \quad \boldsymbol{C} = \begin{bmatrix} \boldsymbol{C}_w & \boldsymbol{I}_{3\times 3} \end{bmatrix} \tag{6.33}$$

And the gain matrix $\boldsymbol{K}_0$ being defined as:

$$\boldsymbol{K}_0(\boldsymbol{\omega}) = \begin{bmatrix} \boldsymbol{K}_1(\boldsymbol{\omega}) \\ \boldsymbol{K}_2 \end{bmatrix} \tag{6.34}$$

Reformulating the body fixed accelerations to:

$$\boldsymbol{M}\tilde{\boldsymbol{\nu}} = -\boldsymbol{D}\tilde{\boldsymbol{\nu}} - \boldsymbol{R}^T(\psi)\tilde{\boldsymbol{z}} \tag{6.35}$$

With $\tilde{\boldsymbol{z}} = \boldsymbol{K}_4\tilde{\boldsymbol{y}} - \tilde{\boldsymbol{b}}$. The stability can then be determined using the Kalman-Yakubovich-Popov lemma, which states that:

Lemma 6.1. *Let $\boldsymbol{Z}(s) = \boldsymbol{C}(s\boldsymbol{I} - \boldsymbol{A})^{-1}\boldsymbol{B}$ be an $m \times m$ transfer function matrix, where $\boldsymbol{A}$ is Hurwitz, $(\boldsymbol{A}, \boldsymbol{B})$ is controllable and $(\boldsymbol{A}, \boldsymbol{C})$ is observable. Then $\boldsymbol{Z}(s)$ is strictly positive real if and only if there exist positive definite matrices $\boldsymbol{P} = \boldsymbol{P}^T$ and $\boldsymbol{Q} = \boldsymbol{Q}^T$ such that:*

$$\boldsymbol{P}\boldsymbol{A} + \boldsymbol{A}^T\boldsymbol{P} = -\boldsymbol{Q} \tag{6.36}$$

$$\boldsymbol{B}^T\boldsymbol{P} = \boldsymbol{C} \tag{6.37}$$

This can be used to determine stability in a Lyapunov sense. If the gains are designed so they yield the matrix $\boldsymbol{A}$ Hurwitz and the pairs $(\boldsymbol{A}, \boldsymbol{B})$ and $(\boldsymbol{A}, \boldsymbol{B})$ controllable and observable, then the system is stable according to the following. Consider the positive definite Lyapunov function candidate based on the *pseudo*-kinetic energy:

$$V = \tilde{\boldsymbol{\nu}}^T\boldsymbol{M}\tilde{\boldsymbol{\nu}} + \tilde{\boldsymbol{x}}^T\boldsymbol{P}\tilde{\boldsymbol{x}} \tag{6.38}$$

Derived along the trajectories of $\tilde{\boldsymbol{\nu}}$ and $\tilde{\boldsymbol{x}}$, gives the following Lyapunov derivative:

$$\dot{V} = \begin{bmatrix} \frac{\partial V}{\partial \tilde{\boldsymbol{\nu}}} & \frac{\partial V}{\partial \tilde{\boldsymbol{x}}} \end{bmatrix} \begin{bmatrix} -\boldsymbol{M}^{-1}\boldsymbol{D}\tilde{\boldsymbol{\nu}} - \boldsymbol{R}^T(\psi)\tilde{\boldsymbol{z}} \\ \boldsymbol{A}\tilde{\boldsymbol{x}} + \boldsymbol{B}\boldsymbol{R}(\psi)\tilde{\boldsymbol{\nu}} \end{bmatrix} \tag{6.39}$$

Which then equals:

$$\begin{aligned} \dot{V} = &-2\tilde{\boldsymbol{\nu}}^T\boldsymbol{D}\tilde{\boldsymbol{\nu}} - 2(\tilde{\boldsymbol{\nu}}^T\boldsymbol{R}^T(\psi)\tilde{\boldsymbol{z}}) + \tilde{\boldsymbol{x}}^T(\boldsymbol{P}\boldsymbol{A} + \boldsymbol{P}\boldsymbol{A})\tilde{\boldsymbol{x}} \\ &+ 2\tilde{\boldsymbol{x}}^T\boldsymbol{P}\boldsymbol{B}\boldsymbol{R}(\psi)\tilde{\boldsymbol{\nu}} \end{aligned} \tag{6.40}$$

The last term of (6.40) can be transposed as the outcome is a number, thus giving:

$$2(\tilde{\boldsymbol{x}}^T \boldsymbol{PBR}(\psi)\tilde{\boldsymbol{\nu}})^T = 2(\tilde{\boldsymbol{\nu}}^T \boldsymbol{R}^T(\psi)\boldsymbol{B}^T \boldsymbol{P}\tilde{\boldsymbol{x}}) \tag{6.41}$$

Using the Kalman-Yakubovich-Popov lemma, the derivative of the Lyapunov function then becomes:

$$\dot{V} = -2\tilde{\boldsymbol{\nu}}^T \boldsymbol{D}\tilde{\boldsymbol{\nu}} - \tilde{\boldsymbol{x}}^T \boldsymbol{Q}\tilde{\boldsymbol{x}} \tag{6.42}$$

Which indeed is negative definite, thus yielding the system Uniformally Global Exponential Stable (as the angular transformation $\boldsymbol{R}(\psi)$ is time dependent).

6.1.3 Gain Determination and Wave Filtering

The last thing to determine is the gains of the system. The stability analysis will hold, as long as the gains fulfil the Kalman-Yakubovich-Popov lemma in 6.1. In the stability analysis, the system was put on state space form and the gains of $\boldsymbol{K}_i$, can be determined from the requirements, that $\boldsymbol{A}$ is Hurwitz, $(\boldsymbol{A}, \boldsymbol{C})$ is observable and $(\boldsymbol{A}, \boldsymbol{B})$ is controllable.

As the systems in (6.29) describe 3 decoupled systems for surge, sway and yaw motion, the gain structure suggests 3 decoupled transfer functions. This calls for gain matrices that are diagonal as the systems are completely decoupled. Thus the gains are defined as:

$$\boldsymbol{K}_1(\boldsymbol{\omega}) = \begin{bmatrix} \mathrm{diag}\{K_{11}(\omega_{o,1}), K_{11}(\omega_{o,2}), K_{13}(\omega_{o,3})\} \\ \mathrm{diag}\{K_{14}(\omega_{o,1}), K_{15}(\omega_{o,2}), K_{16}(\omega_{o,3})\} \end{bmatrix} \tag{6.43}$$

$$\boldsymbol{K}_2 = \mathrm{diag}\{K_{21}, K_{22}, K_{23}\} \tag{6.44}$$

$$\boldsymbol{K}_3 = \mathrm{diag}\{K_{31}, K_{32}, K_{33}\} \tag{6.45}$$

$$\boldsymbol{K}_4 = \mathrm{diag}\{K_{41}, K_{42}, K_{43}\} \tag{6.46}$$

The desired transfer function is given in (6.22) which is depicted on figure 6.3 where the blue line represents the desired notch and low-pass characteristics to properly filter out the second order wave frequency. The transfer function of the $\mathcal{H}_2$ block can be described by three decoupled transfer functions. [FG98] derives these to be:

$$\boldsymbol{H}_0(s) = \boldsymbol{C}_0(s\boldsymbol{I} + \boldsymbol{A}_0 - \boldsymbol{K}_0(\boldsymbol{\omega}_0)\boldsymbol{C}_0)^{-1}\boldsymbol{B}_0 \tag{6.47}$$

$$\boldsymbol{H}_B(s) = \boldsymbol{K}_4 + (s\boldsymbol{I} + \boldsymbol{T}^{-1})^{-1}\boldsymbol{K}_3 \tag{6.48}$$

Which according to [Fos11] can be re-written to the following transfer functions based on diagonal structure of the gain matrices:

$$h_i(s) = \frac{s^2 2\lambda_i\omega_{o,i}s + \omega_{o,i}^2}{s^3 + (K_{1(i+3)} + K_{2i} + 2\lambda_i\omega_{o,i})s^2 + (\omega_{o,i}^2 + 2\lambda_i\omega_{o,i}K_{2i} - K_{1i}\omega_{o,i}^2)s + \omega_{o,i}^2 K_{2i}} \tag{6.49}$$

$$h_{B,i}(s) = \frac{s + \frac{1}{T_i} + \frac{K_{3i}}{K_{4i}}}{s + \frac{1}{T_i}} \approx K_{4i}\frac{s + \frac{K_{3i}}{K_{4i}}}{s + \frac{1}{T_i}}, \text{for } T_i \gg 1 \tag{6.50}$$

To achieve the desired shape (6.22), equalling (6.22) and (6.49), the following tuning rules for the gains following 6.1 can be established. These gains will give a strictly positive real system, and thus ensure stability.

$$K_{1i}(\omega_{o,i}) = -2(\zeta_{n,i} - \lambda_i)\frac{\omega_{c,i}}{\omega_{o,i}} \tag{6.51}$$

$$K_{1(i+3)}(\omega_{o,i}) = 2\omega_{o,i}(\zeta_{n,i} - \lambda_i) \tag{6.52}$$

$$K_{2i} = \omega_{c,i} \tag{6.53}$$

This will thus render the system stable.

Through an analysis of the eigenvalues of the system matrix $\boldsymbol{A}$, the matrix can be made Hurwitz by designing the notch filter with a $\zeta_{n,i} = 0.3$ and the cut-off frequency at $\omega_{c,i} = 1.255\omega_{o,i}$, yields eigenvalues with a strict negative real part. Using these gains, the bode plot depicted on figure 6.4 shows the overall system response, with the notch-lowpass configuration is used to filter out the wave response from figure 6.3. As seen, the bode plot shows that the filter is able to filter out the reponse of the waves.

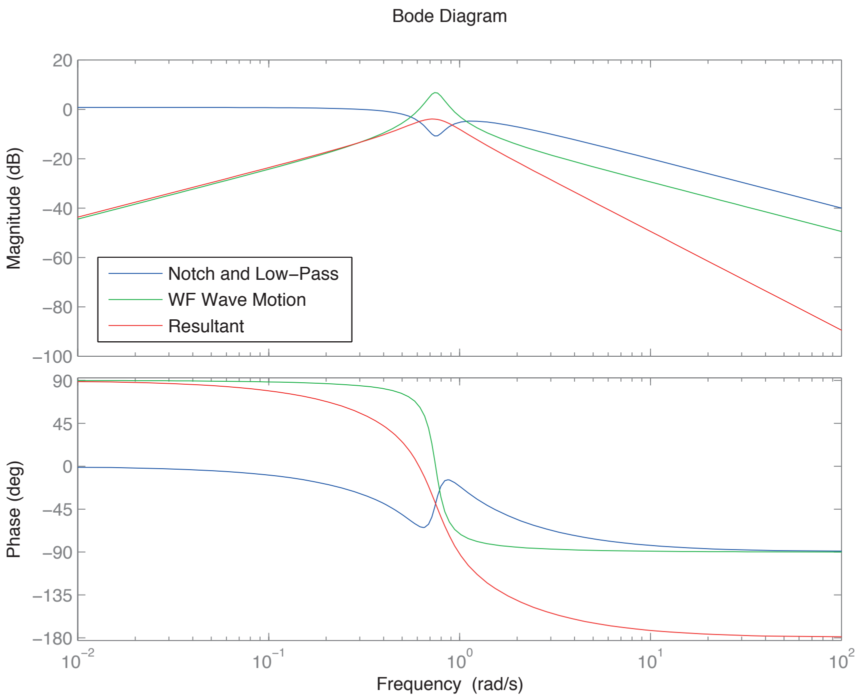

Figure 6.4: Blue being the desired shape of the gains, green the wave response and red the product of the two (the actual output).

6.2 Estimation Conclusion

To verify that the estimator are able to estimate the position, simulations are run in both Matlab and SimFlex. The vessel is tested under two conditions, one with and one without environmental disturbances, but both of them are with added Gaussian noise on the measurements. The variances of the noise are found through tests conducted in [CJsL12], and are given as:

$$\sigma_{gps,X,Y} = 1.0035 \tag{6.54}$$

$$\sigma_{mag} = 4.9 \cdot 10^{-4} \tag{6.55}$$

The simulations are run for 30 minutes with a sampling time of 0.1 Hz. The disturbances are wind, waves and current - as specified in 3.2.

6.2.1 Test using SimFlex

As the DEN-Mark1 simulator provides exact position measurements, these are corrupted with zero-mean Gaussian noise. As seen on figure 6.5 the estimator is able to track the position of the very well, even though the measurements are contaminated with noise. The bias term is depicted on figure 6.7

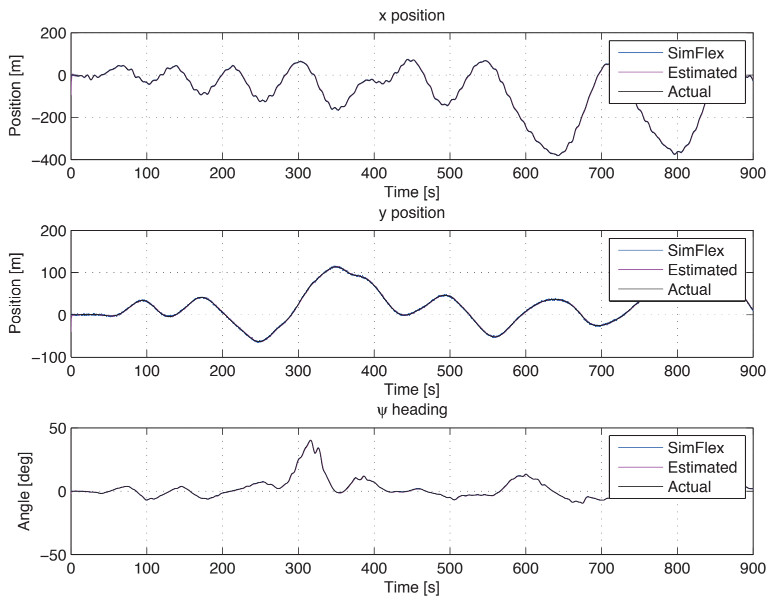

Figure 6.5: The position and heading of the vessel, the blue is the output from DEN-Mark1 and the magenta is the estimate. As seen the estimator is able to track the position of the vessel, even though the system is moved about violently.

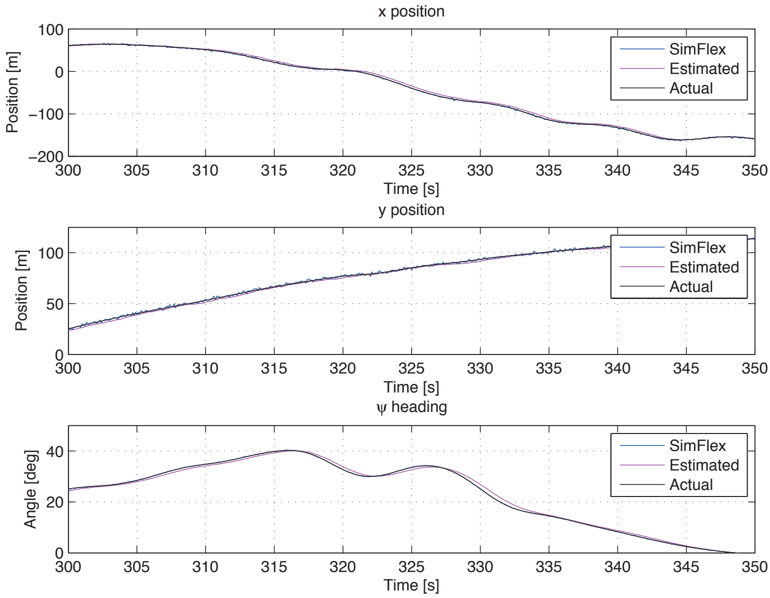

Figure 6.6: A zoomed version of figure 6.5. As seen the observer is able to track the position of the system very well.

As seen on the figures 6.5 and 6.7 the estimator is able to track the position of the vessel, even though the model does not include wave drift or current. This concludes the development of the estimator, and allows for the controller to be developed, based on these estimates.

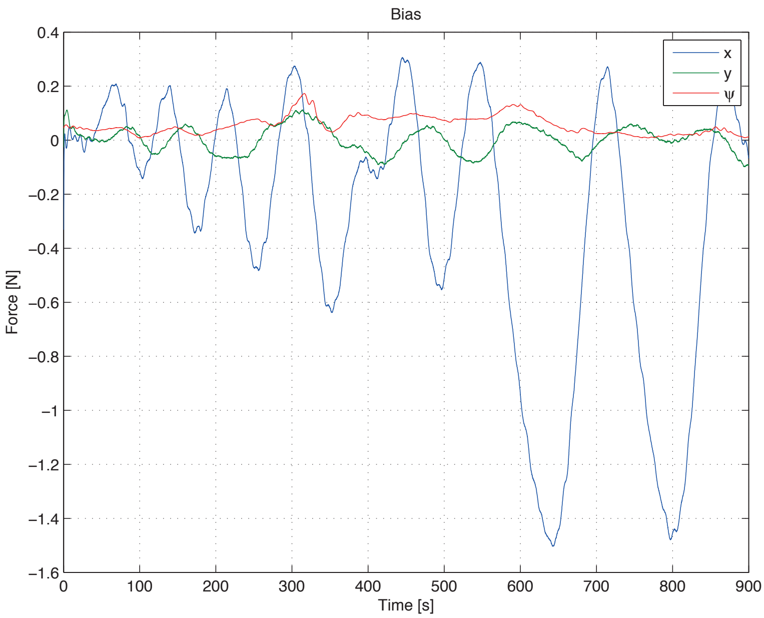

Figure 6.7: The bias term $\boldsymbol{b}$ of the simulation. As seen the bias term is relatively small, this also expresses that the model is accurate. If the bias term $\boldsymbol{b}$ would have been large, the model would have been inaccurate.

Chapter 7

Non-linear Control

This chapter focuses on the development of the non-linear controller. The controller is based on the estimator developed in 6. An advantage of this approach, is that the un-modelled dynamics are driven to zero in the bias term $\boldsymbol{b}$, and will not contribute to the error in the controller. A similar approach is found in [FG98], however, this does not include the wave motions of the vessel, this approach includes the wave motion in the control design, to produce better control signals, as the controller thus acts on these, rather than see them as a disturbance.

7.1 Integrator Backstepping

The main objective of Backstepping, is to remove the *bad* non-linearities, while keeping the *good* ones. An introduction to the theory behind backstepping control can be found in appendix A.

Defining the error variable $\boldsymbol{z}_1$ as the error between the measured and the desired allows for:

$$\boldsymbol{z}_1 = \boldsymbol{y} - \boldsymbol{y}_d \tag{7.1}$$

As was proven in the development of the estimator, this was exponentially stable, and will thus make $\hat{\boldsymbol{y}} \to \boldsymbol{y}$ over time. Replacing $\boldsymbol{y}$ with the estimate $\hat{\boldsymbol{y}}$ will yield an error variable $\boldsymbol{z}_1$ that includes the wave motion. This redefines (7.1) as:

$$\boldsymbol{z}_1 = \hat{\boldsymbol{y}} - \boldsymbol{y}_d \tag{7.2}$$

The virtual control input $\boldsymbol{\phi}$ is chosen as:

$$\boldsymbol{\phi} = \boldsymbol{R}(\psi)\hat{\boldsymbol{\nu}} = \boldsymbol{z}_2 + \boldsymbol{\alpha} \tag{7.3}$$

With the stabilizing function $\boldsymbol{\alpha}$ in (7.3). [FG98] suggests using the following function, with $\boldsymbol{C}_1$ and $\boldsymbol{D}_1$ being positive definite design matrices. The latter is added to damp out the modelling error term $\boldsymbol{K}_2\tilde{\boldsymbol{y}}$:

$$\boldsymbol{\alpha}(\boldsymbol{z}_1) = -\boldsymbol{C}_1\boldsymbol{z}_1 - \boldsymbol{D}_1\boldsymbol{z}_1 + \boldsymbol{y}_d \tag{7.4}$$

Deriving (7.1) gives:

$$\dot{\boldsymbol{z}}_\mathbf{1} = \dot{\boldsymbol{y}} - \dot{\boldsymbol{y}}_\boldsymbol{d} \tag{7.5}$$

Replacing $\dot{\boldsymbol{y}}$ in (7.5) with the derived output of the estimator yields:

$$\dot{\boldsymbol{z}}_\mathbf{1} = \dot{\hat{\boldsymbol{\eta}}} + \boldsymbol{K}_2\tilde{\boldsymbol{y}} - \dot{\boldsymbol{y}}_\boldsymbol{d} \implies \boldsymbol{R}(\psi)\hat{\boldsymbol{\nu}} + \boldsymbol{K}_2\tilde{\boldsymbol{y}} + \boldsymbol{C}_w(\boldsymbol{A}_w\boldsymbol{\xi} + \boldsymbol{K}_1(\boldsymbol{\omega})\tilde{\boldsymbol{y}}) - \dot{\boldsymbol{y}}_\boldsymbol{d} \tag{7.6}$$

The trajectory of the vessel is constant as $\ddot{\boldsymbol{y}}_d, \dot{\boldsymbol{y}}_d = 0$ in station keeping operations. Inserting the virtual control input in (7.6) yields:

$$\dot{\boldsymbol{z}}_\mathbf{1} = \boldsymbol{z}_2 - \boldsymbol{C}_1\boldsymbol{z}_1 - \boldsymbol{D}_1\boldsymbol{z}_1 + \boldsymbol{K}_2\tilde{\boldsymbol{y}} + \boldsymbol{C}_w(\boldsymbol{A}_w\boldsymbol{\xi} + \boldsymbol{K}_1(\boldsymbol{\omega})\tilde{\boldsymbol{y}}) \tag{7.7}$$

Having defined the first error variable, the second can be solved for in (7.3) and gives:

$$\boldsymbol{z}_2 = \boldsymbol{R}(\psi)\hat{\boldsymbol{\nu}} - \boldsymbol{\alpha} \tag{7.8}$$

Given that $\dot{\boldsymbol{R}}(\psi) = \boldsymbol{R}(\psi)\boldsymbol{S}(r)$ as derived in appendix C, the following derivative of $\boldsymbol{z}_2$ can be found:

$$\begin{aligned}
\dot{\boldsymbol{z}}_2 &= \boldsymbol{R}(\psi)\boldsymbol{S}(r)\hat{\boldsymbol{\nu}} + \boldsymbol{R}(\psi)\dot{\hat{\boldsymbol{\nu}}} - \dot{\boldsymbol{\alpha}} &(7.9)\\
&= \boldsymbol{R}(\psi)\boldsymbol{S}(\psi)\hat{\boldsymbol{\nu}} + \boldsymbol{R}(\psi)\dot{\hat{\boldsymbol{\nu}}} + \boldsymbol{C}_1\dot{\boldsymbol{z}}_1 + \boldsymbol{D}_1\dot{\boldsymbol{z}}_1 + \ddot{\boldsymbol{y}}_d &(7.10)
\end{aligned}$$

Inserting the estimator model $\dot{\hat{\boldsymbol{\nu}}}$ and $\dot{\boldsymbol{z}}_1$ into (7.10) yields the following:

$$\begin{aligned}
\dot{\boldsymbol{z}}_2 = {}& \boldsymbol{R}(\psi)\boldsymbol{S}(r)\hat{\boldsymbol{\nu}} + \boldsymbol{R}(\psi)\boldsymbol{M}^{-1}(-\boldsymbol{D}\hat{\boldsymbol{\nu}} + \boldsymbol{R}^T(\psi)\boldsymbol{K}_2\hat{\boldsymbol{b}} + \boldsymbol{R}^T(\psi)\boldsymbol{K}_4\tilde{\boldsymbol{y}} + \boldsymbol{\tau})\\
&- (\boldsymbol{C}_1 + \boldsymbol{D}_1)^2\boldsymbol{z}_1 + (\boldsymbol{C}_1 + \boldsymbol{D}_1)\boldsymbol{z}_2 + (\boldsymbol{C}_1 + \boldsymbol{D}_1)(\boldsymbol{C}_w(\boldsymbol{A}_w\boldsymbol{\xi} + \boldsymbol{K}_1(\boldsymbol{\omega})\tilde{\boldsymbol{y}})) \qquad (7.11)
\end{aligned}$$

Collecting terms for notational simplicity:

$$\begin{aligned}
\dot{\boldsymbol{z}}_2 = {}& (\boldsymbol{R}(\psi)\boldsymbol{S}(r)) - \boldsymbol{R}(\psi)\boldsymbol{M}^{-1}\boldsymbol{D})\hat{\boldsymbol{\nu}}\\
&+ \boldsymbol{R}(\psi)\boldsymbol{M}^{-1}(\boldsymbol{R}^T(\psi)\boldsymbol{K}_2)\hat{\boldsymbol{b}}\\
&- (\boldsymbol{C}_1 + \boldsymbol{D}_1)^2\boldsymbol{z}_1 + (\boldsymbol{C}_1 + \boldsymbol{D}_1)\boldsymbol{z}_2\\
&+ ((\boldsymbol{C}_1 + \boldsymbol{D}_1)(\boldsymbol{C}_w(\boldsymbol{A}_w\boldsymbol{\xi} + \boldsymbol{K}_1(\boldsymbol{\omega})) + \boldsymbol{R}^T(\psi)\boldsymbol{K}_4)\tilde{\boldsymbol{y}}\\
&+ \boldsymbol{R}(\psi)\boldsymbol{M}^{-1}\boldsymbol{\tau} \qquad (7.12)
\end{aligned}$$

Thus, selecting an input that cancel the *bad* non-linearities. For simplicity, an expression that resembles that of $\boldsymbol{z}_1$ is wanted, thus choosing the input $\boldsymbol{\tau}$ as:

$$\begin{aligned}
\boldsymbol{R}(\psi)\boldsymbol{M}^{-1}\boldsymbol{\tau} = {}& -((\boldsymbol{R}(\psi)\boldsymbol{M}^{-1} + \boldsymbol{R}(\psi)\boldsymbol{S}(r))\hat{\boldsymbol{\nu}} + \boldsymbol{R}(\psi)\boldsymbol{M}^{-1}\boldsymbol{R}^T(\psi)\boldsymbol{K}_2\hat{\mathrm{b}}\\
&+ \ddot{\boldsymbol{y}}_d - (\boldsymbol{C}_1 + \boldsymbol{D}_1)^2\boldsymbol{z}_1 + (\boldsymbol{C}_1 + \boldsymbol{D}_1)\boldsymbol{z}_2 + \boldsymbol{R}(\psi)\boldsymbol{M}^{-1}\boldsymbol{R}^T\boldsymbol{K}_4\tilde{\boldsymbol{y}}\\
&+ \boldsymbol{z}_1 + (\boldsymbol{C}_2 + \boldsymbol{D}_2)\boldsymbol{z}_2) \qquad (7.13)
\end{aligned}$$

And then inserting (7.13) into (7.11) gives:

$$\dot{\boldsymbol{z}}_2 = -\boldsymbol{z}_1 - (\boldsymbol{C}_2 + \boldsymbol{D}_2)\boldsymbol{z}_2 + (\boldsymbol{C}_1 + \boldsymbol{D}_1)(\boldsymbol{C}_w \boldsymbol{A}_w \hat{\boldsymbol{\xi}} + (\boldsymbol{K}_2 + \boldsymbol{C}_w \boldsymbol{K}_1(\boldsymbol{\omega})))\tilde{\boldsymbol{y}}) \tag{7.14}$$

Which is resemblent to $\dot{\boldsymbol{z}}_1$ in (7.7). If a new state vector $\boldsymbol{z}$ is defined as $\boldsymbol{z} = [\boldsymbol{z}_1^T, \boldsymbol{z}_2^T]^T$, the system can be re-written to:

$$\dot{\boldsymbol{z}} = -(\tilde{\boldsymbol{C}} + \tilde{\boldsymbol{D}} - \tilde{\boldsymbol{I}})\boldsymbol{z} + \tilde{\boldsymbol{W}}_{\boldsymbol{1}}\tilde{\boldsymbol{y}} + \tilde{\boldsymbol{W}}_{\boldsymbol{2}}\hat{\boldsymbol{\xi}} \tag{7.15}$$

With the matrices $\tilde{\boldsymbol{C}}, \tilde{\boldsymbol{D}}$ and $\tilde{\boldsymbol{I}}$ being defined as:

$$\tilde{\boldsymbol{C}} = \begin{bmatrix} \boldsymbol{C}_1 & \boldsymbol{0}_{3\times3} \\ \boldsymbol{0}_{3\times3} & \boldsymbol{C}_2 \end{bmatrix}, \quad \tilde{\boldsymbol{D}} = \begin{bmatrix} \boldsymbol{D}_1 & \boldsymbol{0}_{3\times3} \\ \boldsymbol{0}_{3\times3} & \boldsymbol{D}_2 \end{bmatrix}, \quad \tilde{\boldsymbol{I}} = \begin{bmatrix} \boldsymbol{0}_{3\times3} & -\boldsymbol{I} \\ \boldsymbol{I} & \boldsymbol{0}_{3\times3} \end{bmatrix} \tag{7.16}$$

And the two column matrices $\tilde{\boldsymbol{W}}_{\boldsymbol{1}}$ and $\tilde{\boldsymbol{W}}_{\boldsymbol{2}}$ as:

$$\tilde{\boldsymbol{W}}_{\boldsymbol{1}} = \begin{bmatrix} \boldsymbol{K}_2 + \boldsymbol{C}_w \boldsymbol{K}_1(\boldsymbol{\omega}) \\ (\boldsymbol{C}_1 + \boldsymbol{D}_1)(\boldsymbol{K}_2 + \boldsymbol{C}_w \boldsymbol{K}_1(\boldsymbol{\omega})) \end{bmatrix}, \quad \tilde{\boldsymbol{W}}_{\boldsymbol{2}} = \begin{bmatrix} \boldsymbol{C}_w \boldsymbol{A}_w \\ (\boldsymbol{C}_1 + \boldsymbol{D}_1)\boldsymbol{C}_w \boldsymbol{A}_w \end{bmatrix} \tag{7.17}$$

If (7.15) can be proven stable in a Lyapunov sense, the proposed control strategy is viable, and will provide a stable result.

7.1.1 Stability Analysis

To verify the stability of the controller, a Lyapunov stability analysis is performed. The Lyapunov function candidate $V(\boldsymbol{z}) > 0, \forall z \neq 0$ is defined as:

$$V = \frac{1}{2}\boldsymbol{z}^T\boldsymbol{z} \tag{7.18}$$

With the derivative

$$\dot{V} = V_{\boldsymbol{z}}\dot{\boldsymbol{z}} = -\boldsymbol{z}^T(\tilde{\boldsymbol{C}} + \tilde{\boldsymbol{D}} - \tilde{\boldsymbol{I}})\boldsymbol{z} + \boldsymbol{z}^T\tilde{\boldsymbol{W}}_{\boldsymbol{1}}\tilde{\boldsymbol{y}} + \boldsymbol{z}^T\tilde{\boldsymbol{W}}_{\boldsymbol{2}}\hat{\boldsymbol{\xi}} \tag{7.19}$$

The first term $-\boldsymbol{z}^T(\tilde{\boldsymbol{C}} + \tilde{\boldsymbol{D}} - \tilde{\boldsymbol{I}})\boldsymbol{z}$ is negative definite, due to $\tilde{\boldsymbol{C}}, \tilde{\boldsymbol{D}} > 0$. The term $\boldsymbol{z}^T\tilde{\boldsymbol{I}}\boldsymbol{z} = \boldsymbol{0}$ and will not contribute to the definiteness. However, the two terms $\boldsymbol{z}^T\tilde{\boldsymbol{W}}_{\boldsymbol{1}}\tilde{\boldsymbol{y}}$ and $\boldsymbol{z}^T\tilde{\boldsymbol{W}}_{\boldsymbol{2}}\hat{\boldsymbol{\xi}}$ cannot be interpreted to be negative definite intuitively. However, the form of the two matrices $\tilde{\boldsymbol{W}}_1$ and $\tilde{\boldsymbol{W}}_2$, given as in (7.17) are to be made negative definite to ensure stability.

To render these two terms negative definite, the first term $-\boldsymbol{z}^T(\tilde{\boldsymbol{C}} + \tilde{\boldsymbol{D}} - \tilde{\boldsymbol{I}})\boldsymbol{z}$ should dominate $\tilde{\boldsymbol{W}}_1$ and $\tilde{\boldsymbol{W}}_2$ to guarantee stability. This can be achieved by designing the two gain matrices $\boldsymbol{C}_2$ and $\boldsymbol{D}_2$ to be larger than $\boldsymbol{C}_1$ and $\boldsymbol{D}_1$. To give a qualitative measure of how large they should be, the norm of the matrices are used to compute a scaling factor. The $\boldsymbol{C}_1$ and $\boldsymbol{D}_1$ matrices can be computed as:

$$\boldsymbol{C}_1 = 2\boldsymbol{I}_{3\times3}||(\boldsymbol{K}_2 + \boldsymbol{C}_w\boldsymbol{K}_1(\boldsymbol{\omega}))|| \tag{7.20}$$

$$\boldsymbol{D}_1 = 2\boldsymbol{I}_{3\times3}||(\boldsymbol{K}_2 + \boldsymbol{C}_w\boldsymbol{K}_1(\boldsymbol{\omega}))|| \tag{7.21}$$

Which are then gained according to the norm of $\tilde{\boldsymbol{W}}_{\boldsymbol{1}}$, as this is larger than the norm of $(\boldsymbol{C}_1 + \boldsymbol{D}_1)\boldsymbol{C}_w\boldsymbol{A}_w$. Thus:

$$\boldsymbol{C}_2 = \boldsymbol{C}_1 ||(\boldsymbol{C}_1 + \boldsymbol{D}_1)(\boldsymbol{K}_2 + \boldsymbol{C}_w\boldsymbol{K}_1(\boldsymbol{\omega}))|| \tag{7.22}$$

$$\boldsymbol{D}_2 = \boldsymbol{D}_1 ||(\boldsymbol{C}_1 + \boldsymbol{D}_1)(\boldsymbol{K}_2 + \boldsymbol{C}_w\boldsymbol{K}_1(\boldsymbol{\omega}))|| \tag{7.23}$$

This will ensure stability, as these two matrices will dominate the two other. As $\dot{V}$ is negative definite through this scaling - the system has been proven to be Globally Exponential Stable (GES). The 3 phases on figure 7.1 depicts that the three error signals converges towards the equilibrium. The tests conducted are on the control system simulated in Matlab for 100 seconds, with no disturbances on the measurements, and a $\boldsymbol{y}_d$ given as:

$$\boldsymbol{y}_d(k) = [0, 0, 0]^T, \text{ for } k = 0, \dots, 300 \tag{7.24}$$

$$\boldsymbol{y}_d(k) = [5, 5, 2]^T, \text{ for } k = 300, \dots, 1000 \tag{7.25}$$

indsæt konstanter

The reference are smoothed out by a low pass filter with , as a step input is too violent for

Thus, the system have been simulated with a step input. If noise is added, the phase plot on figure 7.2 is produced. As seen, the error variables also converge to the equilibrium, or close to, even though the noise perturbs the system. The reason for the error variables being larger in along the $\boldsymbol{z}_2$ axis, stems from the definition of this. As $\boldsymbol{z}_2$ is a scaled version of $\boldsymbol{z}_1$ through the gain matrices $\boldsymbol{C}_1$ and $\boldsymbol{D}_1$.

This concludes the development of the controller. The following section will show a proof-of-concept simulation in Matlab, to show that the system works as intended.

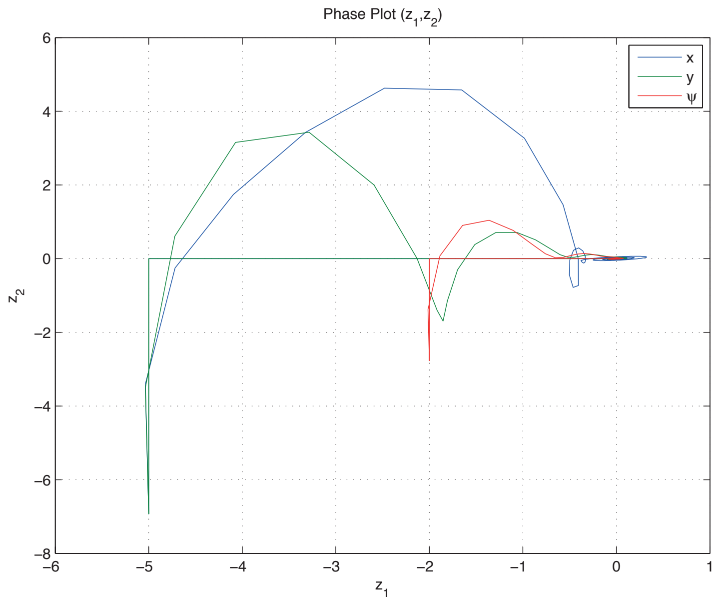

Figure 7.1: Phase plot of the two error variables $\boldsymbol{z}_1$ and $\boldsymbol{z}_2$. Simulated in Matlab, with no noise, and a $\boldsymbol{y}_d$ as in (7.25).

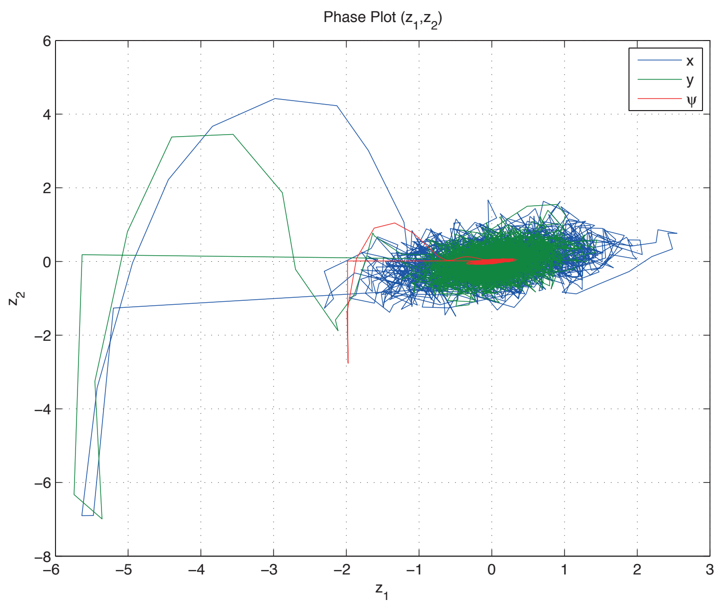

Figure 7.2: Phase plot of the two error variables $\boldsymbol{z}_1$ and $\boldsymbol{z}_2$. Simulated in Matlab, with added noise, and a $\boldsymbol{y}_d$ as in (7.25).

7.2 Control Allocation

This section will describe the development of an on-line thrust allocating module - that in real-time is able to compute the most optimal thrust allocation. The reason for an on-line module compared to a lookup table, is that the loss of a thruster can be implemented directly in the controller by changing the weights of gain matrices.

7.2.1 Thruster Configuration

As seen in equation (7.13) the input to the system is termed as a force $\boldsymbol{\tau}$ with a component in the x-, y-direction as well as moment about the z-axis. However, the shuttle tanker is mounted with 6 individual thrusters, which for a 3-DOF controller could yield an infinite amount of configurations as the ship is over-actuated. The goal is to find a solution that are as efficient as possible.

Table 7.1 describes the characteristics of the thruster configuration aboard the vessel - with the numeration and naming as on figure 7.3. The offsets of the thrusters are normalized with the length between the perpendiculars L_{pp} and the thrust have been normalized with respect to the largest possible thrust delivered to the controller $\max\{F_{main}\}$.

Fig. #	Description	x-offset/L_{pp} [-]	y-offset/L_{pp} [-]	Max/Min [-]
# 1	Main Propeller	-0.481	0	1/-0.8133
# 2	Stern Tunnel Thruster	-0.416	0	0.191/-0.191
# 3	Stern Azimuth	-0.321	0	0.28/0
# 4	Bow Tunnel Thruster 1	0.477	0	0.191/-0.191
# 5	Bow Tunnel Thruster 2	0.492	0	0.191/-0.191
# 6	Bow Azimuth	0.385	0	0.28/0

Table 7.1: Table of thruster configuration aboard the used vessel.

The mapping from $\boldsymbol{\tau}$ to a thrust $\boldsymbol{f}$ and angle $\boldsymbol{\alpha}$ of the individual thrusters settings can be done through the following matrix:

$$\boldsymbol{\tau}_{ctrl} = \boldsymbol{T}(\boldsymbol{\alpha})\boldsymbol{f} \tag{7.26}$$

Where the matrix $\boldsymbol{T}$ denotes the mapping from a desired force to the thrusters. This matrix is constructed from figure 7.3 and is a function of the forces and moments acting on the vessel, given as:

$$\boldsymbol{T}(\boldsymbol{\alpha}) = \begin{bmatrix} 1 & 0 & 0 & 0 & \cos(\alpha_1) & \cos(\alpha_2) \\ 0 & 1 & 1 & 1 & \sin(\alpha_1) & \sin(\alpha_2) \\ 0 & l_{stern} & l_{bow1} & l_{bow2} & l_{az-stern}\sin(\alpha_1) & l_{az-bow}\cos(\alpha_2) \end{bmatrix} \tag{7.27}$$

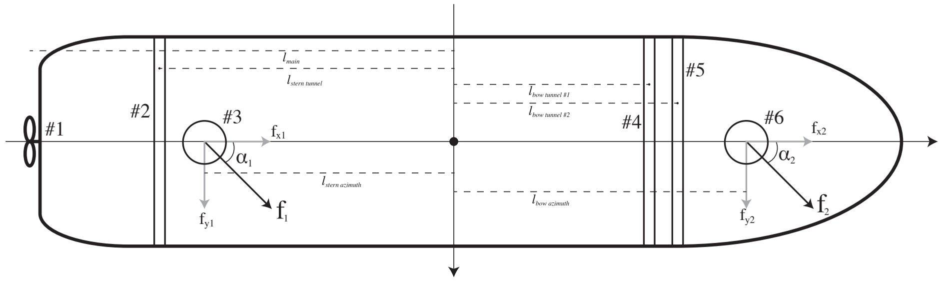

Figure 7.3: Thruster configuration of the shuttle tanker. The drawing is not to scale, but serves as a reference to where the individual thrusters are located.

The easy solution would be to solve the equation in 7.26, however, as $\boldsymbol{T}(\boldsymbol{\alpha})$ is not square, the solution is not straight forward. A proposal to a solution could be to minimize a quadratic function with respect to the change in thrust and angle.

7.2.2 Cost Function and Constraints

As it is undesirable to change the thrust for each thruster too much at each time step, the thrust allocation should minimize the change between each time step, in this way, the optimization algorithm will ensure that the change at each iteration is sufficiently small, and should ensure convergence towards a minima. This condition also holds the physical property that the thrust is unable to change from 0 to 800 kN in one iteration.

This redefines the thrust $\boldsymbol{f}$ and angle $\boldsymbol{\alpha}$ defined in (7.27) to:

$$\boldsymbol{f} = \boldsymbol{f}_0 + \Delta \boldsymbol{f} \tag{7.28}$$

$$\boldsymbol{\alpha} = \boldsymbol{\alpha}_0 + \Delta \boldsymbol{\alpha} \tag{7.29}$$

The force components in (7.27) are linear and thus fairly easy to solve, the angular components are not, and one solution will be hard to determine. This becomes evident on figure 7.4, 7.5 and 7.6 where the force and moment are plotted for various angles of the azimuth thrusters. From this it is desirable only to minimize the change in angle, as a minimized angle would try to make the thrusters converge to zero degrees, and thereby not produce any moment.

A term $\max\{\Delta \boldsymbol{f}\}$ is added to minimize the biggest force, and thereby try to use the thrusters as little as possible. With this in mind, the following convex cost function in (7.30) is proposed:

$$\mathcal{J} = \boldsymbol{f}^T \boldsymbol{Q} \boldsymbol{f} + \Delta \boldsymbol{\alpha}^T \boldsymbol{P} \Delta \boldsymbol{\alpha} + \max\{\Delta \boldsymbol{f}\} \tag{7.30}$$

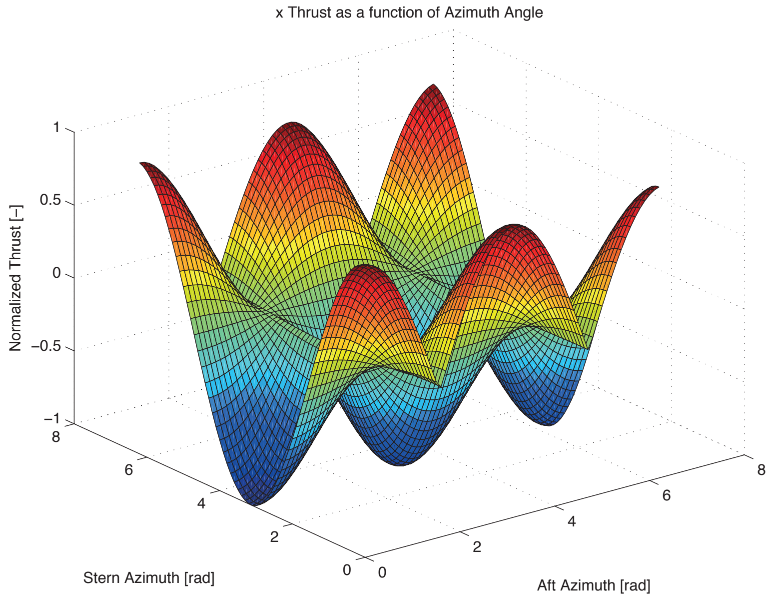

Figure 7.4: Normalized x-thrust from the azimuth thrusters as a function of the angle.

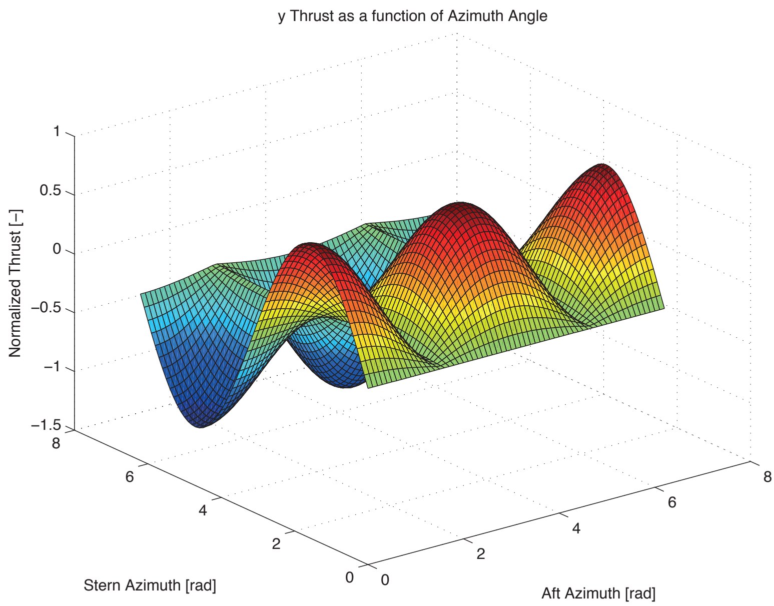

Figure 7.5: Normalized y-thrust from the azimuth thrusters as a function of the angle.

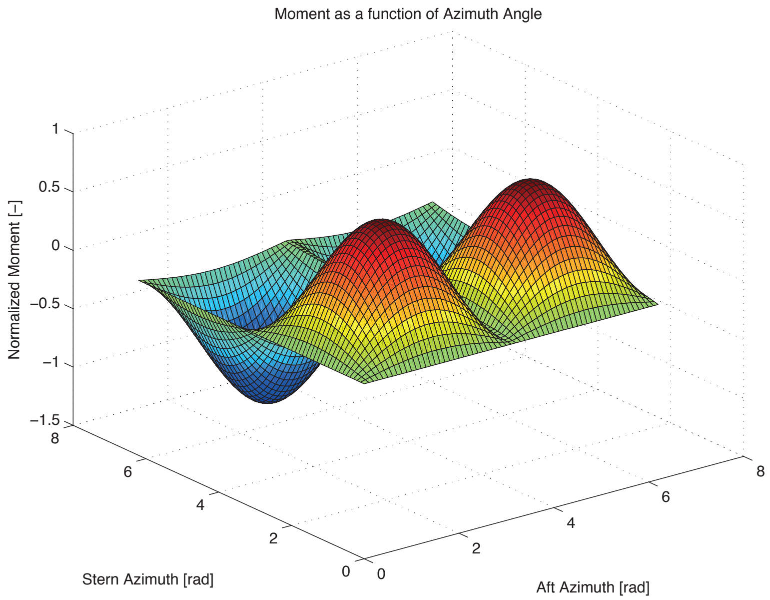

Figure 7.6: Normalized moment from the azimuth thrusters as a function of the angle.

A quadratic cost function are in [NW99] defined as convex if the matrices $\boldsymbol{Q}$ and $\boldsymbol{P}$ are positive definite matrices. As these are design matrices, they are designed as $\boldsymbol{Q} = \boldsymbol{Q}^T > 0$ and $\boldsymbol{P} = \boldsymbol{P}^T > 0$, and contains penalizing constants on the diagonal. The constraints then take the form:

$$\boldsymbol{T}(\boldsymbol{\alpha}_0)(\boldsymbol{f}_0 + \Delta f) = \boldsymbol{\tau} \tag{7.31}$$

$$\boldsymbol{f}_{min} - \boldsymbol{f}_0 \leq \Delta \boldsymbol{f} \leq \boldsymbol{f}_{max} - \boldsymbol{f}_0 \tag{7.32}$$

$$\boldsymbol{\alpha}_{min} - \boldsymbol{\alpha}_0 \leq \Delta \boldsymbol{\alpha} \leq \boldsymbol{\alpha}_{max} - \boldsymbol{\alpha}_0 \tag{7.33}$$

The equality constraint in (7.35) can however be hard to reach exactly, and an exact solution would be too time consuming to compute, so a slack variable $\boldsymbol{s}$ is added to both the constraint (7.35) and the cost function (7.30), thus reaching:

$$\mathcal{J} = \boldsymbol{f}^T \boldsymbol{Q} \boldsymbol{f} + \Delta \boldsymbol{\alpha}^T \boldsymbol{P} \Delta \boldsymbol{\alpha} + \boldsymbol{s}^T \boldsymbol{R} \boldsymbol{s} + \max\{\Delta \boldsymbol{f}\} \tag{7.34}$$

Subject to the following constraints:

$$\boldsymbol{s} + \boldsymbol{T}(\boldsymbol{\alpha}_0)(\boldsymbol{f}_0 + \Delta f) = \boldsymbol{\tau} \tag{7.35}$$

$$\boldsymbol{f}_{min} - \boldsymbol{f}_0 \leq \Delta \boldsymbol{f} \leq \boldsymbol{f}_{max} - \boldsymbol{f}_0 \tag{7.36}$$

$$\boldsymbol{\alpha}_{min} - \boldsymbol{\alpha}_0 \leq \Delta \boldsymbol{\alpha} \leq \boldsymbol{\alpha}_{max} - \boldsymbol{\alpha}_0 \tag{7.37}$$

The purpose of the cost function is then to minimize the thrust output $\boldsymbol{f}_0 + \Delta \boldsymbol{f}$ and the change in angle $\Delta \boldsymbol{\alpha}$.

7.2.3 Verification

Even though the cost function in (7.34) is convex solutions for a reference thrust vector $\boldsymbol{\tau}$ that fluctuates, have made the problem unsolvable. However, if the noise is removed from the system, the proposed algorithm is able to provide the following solution for the $\boldsymbol{y}_d$ given in (7.39). The results presented here, are with no noise on the measurements and a very small step size. The control signal is computed with the algorithm proposed in (7.13), and both the wind $\boldsymbol{\tau}_{wind}$ and current $\boldsymbol{\tau}_{current}$ are fed forward.

$$\boldsymbol{y}_d = [0, 0, 0]^T, \text{for } k = 0 \ldots 300 \tag{7.38}$$

$$\boldsymbol{y}_d = [0.01, 0.01, 0]^T, \text{for } k = 301 \ldots 1000 \tag{7.39}$$

The results show that the thrust allocator is able to provide a solution for the given configuration. However, the steps are small - and tests in Matlab and DEN-Mark1 have shown that the allocator cannot cope with the changes induced on the vessel with the simulation parameters described in 3.2. However, the optimizer have produced the plots in figure 7.7 and 7.8, that depicts the thruster mapping between the control signal and a figure of the comparison between the demanded and delivered thrust.

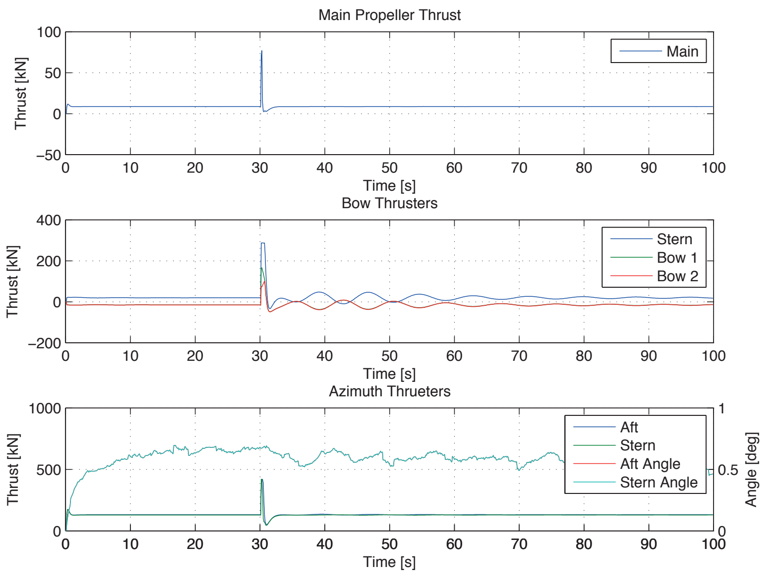

Figure 7.7: Resulting thrust mapping from the optimization algorithm.

7.2.4 Concluding Remarks

Even though the optimiser have been implemented, tests have shown that the algorithm tends to become affine when noise is introduced and when the changes in

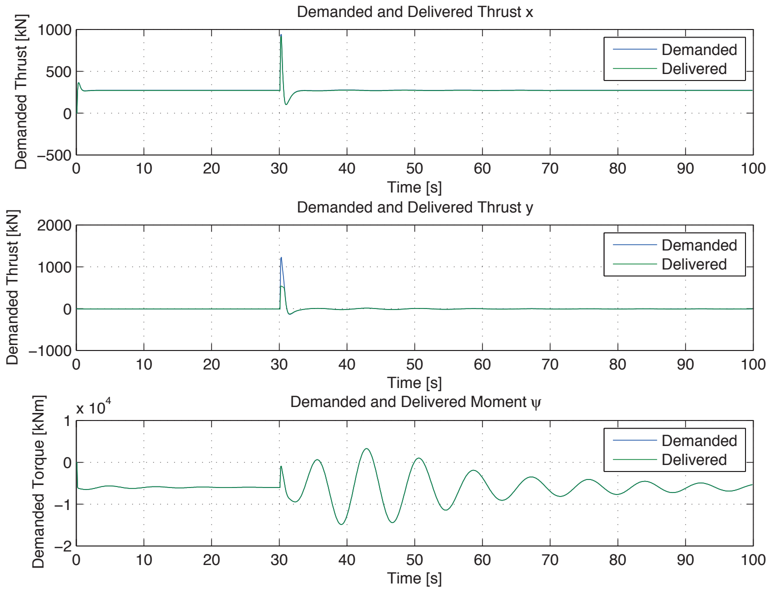

Figure 7.8: Demanded and delivered thrust.

the control signal are large (jumps from 0 to 10^5 to in two samples), which is clear, as the controller is not saturated and the non-linearity of the controller allows for fast and large changes. A way to cope with this, could be to implement an input shaper (or a low pass filter), however, stability cannot be guaranteed.

7.3 Control Conclusion

The controller have been simulated in Matlab. However, a static tests of the system provides no answer on how the controller responds, so the controller have been simulated with a step input defined as.

$$\boldsymbol{y}_d(k) = [10, 10, 2]^T, \text{ for } k = 500, \ldots, 5000 \tag{7.40}$$

$$\boldsymbol{y}_d(k) = [0, -15, 2]^T, \text{ for } k = 5000, \ldots, 7500 \tag{7.41}$$

$$\boldsymbol{y}_d(k) = [0, -15, 0]^T, \text{ for } k = 7500, \ldots, 10000 \tag{7.42}$$

The input have been shaped using a second order low-pass filter, with a damping coefficient $\lambda = 10$ and a natural frequency of $\omega_n = 1$. When simulated with and without noise, the following position and phase plots are produced for the systems. The input generated is not limited, and is fed directly to the observer, so no saturation elements are enforced on it. This is not viable in a real system, as the engines are not able to change thrust that fast.

The plots on figure 7.9 and 7.10 are noiseless simulations with the proposed controller and estimator. And the plots on figure 7.11 and 7.12 are with added Gaussian noise. The variance of the noise is given in (6.54) and (6.55) for the GPS and the compass respectively.

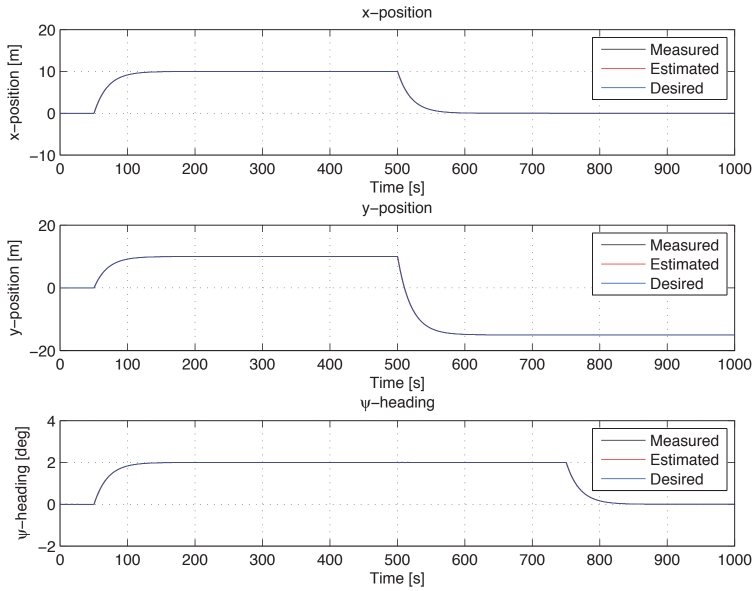

Figure 7.9: The position of the vessel with the proposed controller, the simulation is noiseless and the desired trajectory $\boldsymbol{y}_d$ is a lowpass filtered version of that in (7.42).

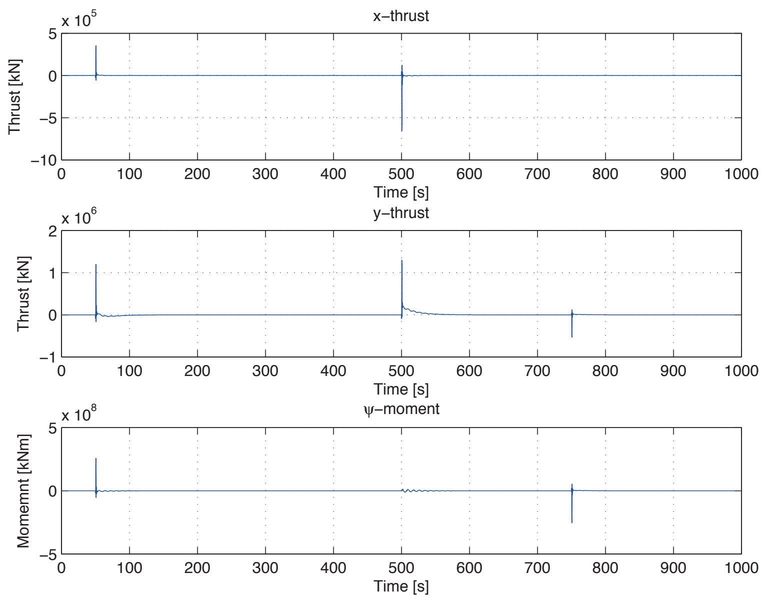

Figure 7.10: The thrust inputs to the vessel with the proposed controller. This simulation is noiseless.

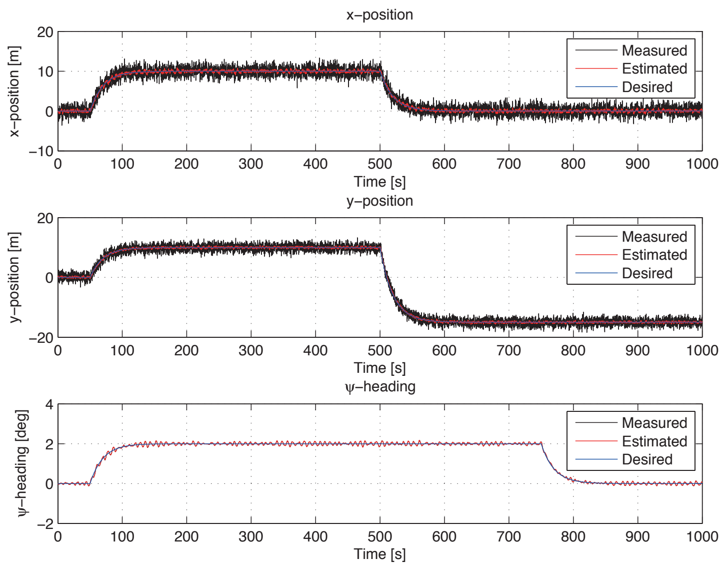

Figure 7.11: The position of the vessel with the proposed controller, the simulation is with added Gaussian noise on the measurements $\boldsymbol{y}$ and the desired trajectory $\boldsymbol{y}_d$ is a lowpass filtered version of (7.42).

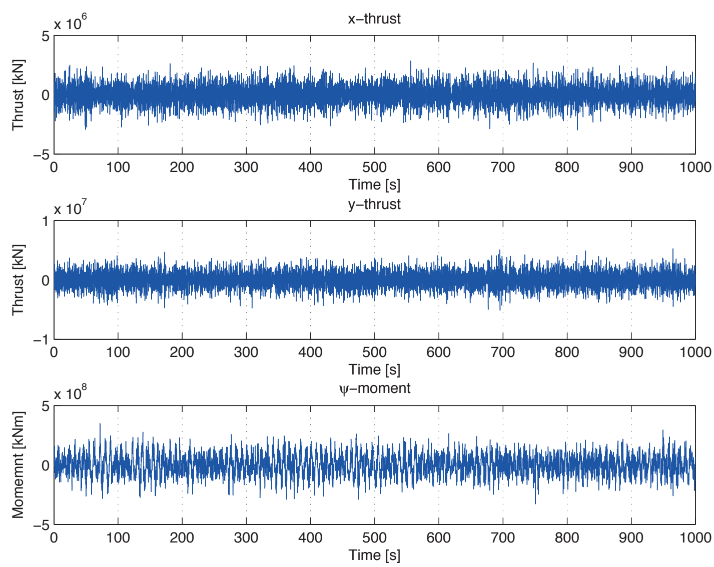

Figure 7.12: The thrust inputs to the vessel with the proposed controller. This simulation is with added Gaussian noise on the measurements $\boldsymbol{y}$.

Chapter 8
Verification

The developed controller is tested against that of FORCE TECHNOLOGY . The performance criteria are as specified in 3.3. As the software implementation of the proposed controller in DEN-Mark1 have yielded problematic, the linear PID controller have been implemented in Matlab, and the comparison and thus verification of the proposed controller will be carried out on the model used in the estimator in 6.

The linear controller used at FORCE TECHNOLOGY does not contain any cross terms in the gain matrices, and will thus be implemented as:

$$\boldsymbol{\tau}_k = \boldsymbol{K}_p \boldsymbol{z}_1 + \boldsymbol{K}_i \sum_{i=0}^{k} \boldsymbol{z}_1 + \boldsymbol{K}_d \dot{\boldsymbol{z}}_1 + \boldsymbol{\tau}_{wind} \tag{8.1}$$

With $\boldsymbol{K}_{p,i,d}$ being diagonal matrices of positive gain elements of the linear controller.

As the tests otherwise would have been conducted with a controllers that could tend towards infinity to acquire the desired position of the vessel, a hard coded saturation element have been enforced on both the controllers, with the highest possible forward and reverse thrust as well as the highest positive and negative torque set as the limits. This form of test is not ideal, it does however point towards the performance of the controllers, and as both of them are tested under the same circumstances, provides a reasonable comparison.

8.1 Performance of the Estimator

The estimator have been simulated. The data is from the simulation with an angle of attack of -15 degrees, and the plot on figure 8.1 depicts the vessels measured position as well as the estimated.

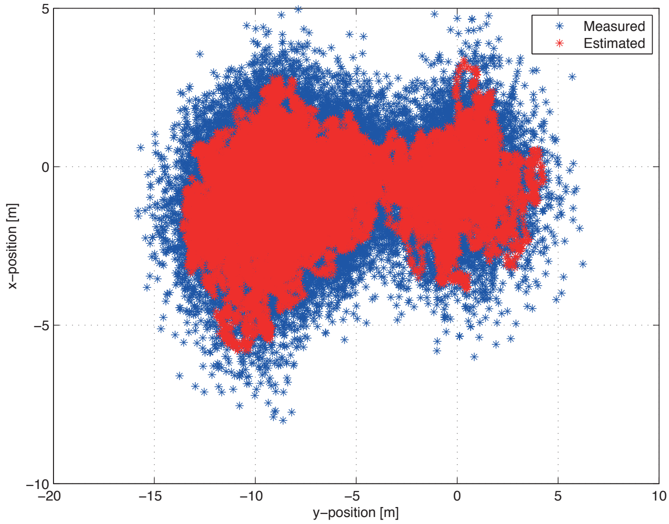

Figure 8.1: A plot of the position estimate for the -15 degree test. As seen, the estimator clearly provides filtering, and the estimates are better than the original GPS measurement. The

8.2 Deviation Plots

The deviation plots for the proposed control strategy as well as the original controller are presented here. A description of the plots and how they are interpreted can be found in 3.3. The two plots 8.2 and 8.3 depicts the total deviation from all the negative and positive angle tests combined.

8.3 Performance of the Controller

Another measure of performance is the performance index. The function used to compute these, given in (3.1), takes into account the biggest deviation from the origin, as well as the highest input. These weights are then multiplied with the position and thrust at each time step - and will thus provide a performance of the individual tests.

These are listed in the table below.

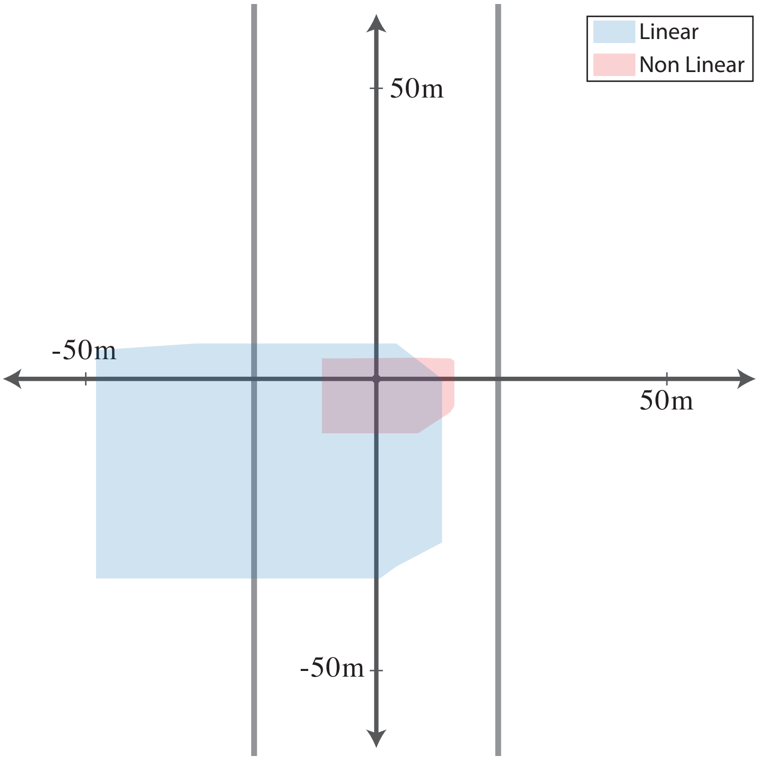

Figure 8.2: A plot of the positive angles of attack. The non-linear controller provides better results. As seen in 8.1 the performance is a lot better when looking at the maximum deviation.

Test β	$\mathcal{J}$-PID-Control	$\mathcal{J}$-Non-linear	$\max_{PID}\{\lvert\boldsymbol{y}\rvert\}$	$\max_{NL}\{\lvert\boldsymbol{y}\rvert\}$
$-15°$	75789	125390	$(44.86, 17.00, 83.41)$	$(5.80, 13.61, 0.51)$
$-10°$	74601	118500	$(20.72, 25.14, 68.56)$	$(5.43, 17.12, 0.57)$
$-5°$	66468	118326	$(38.17, 50.89, 35.80)$	$(5.56, 11.81, 0.57)$
$0°$	43554	117259	$(415.30, 59.78, 0.63)$	$(4.30, 11.85, 0.53)$
$5°$	82611	119167	$(34.35, 48.20, 19.38)$	$(4.78, 8.78, 0.44)$
$10°$	79118	117344	$(32.29, 31.13, 43.78)$	$(5.35, 9.36, 0.53)$
$15°$	95514	117817	$(28.15, 11.30, 57.15)$	$(4.65, 13.43, 0.67)$

Table 8.1: Performance index or the individual tests. The performance function $\mathcal{J}$ is given in (3.1). The higher the performance index, the better the controller. The non-linear controller outperforms the linear counterpart. Generally, the linear controller performs better for positive angles of attack.

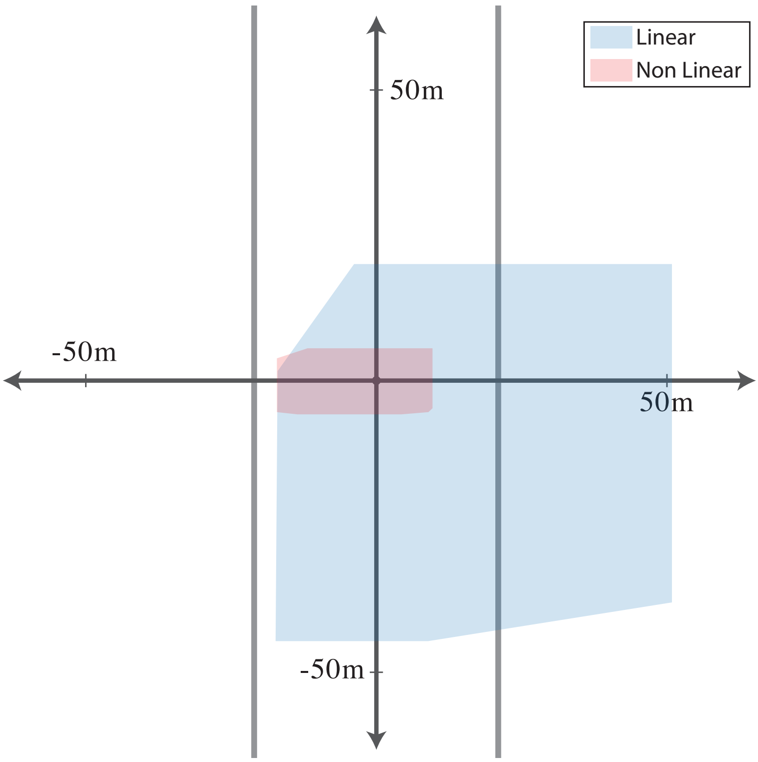

Figure 8.3: A plot of the negative angles of attack. The linear controller has a much higher deviation from the original point than the non-linear counterpart.

Chapter 9 Conclusion

This project have documented the development of a non-linear controller to be used aboard a shuttle tanker. The controller is non-linear of nature, and should therefore provide a response that are better than the linear counterpart currently being used at FORCE TECHNOLOGY .

The proposed algorithm are based on 3 parts, a non-linear model, a non-linear estimator and a non-linear controller. The model is derived for ships in station keeping operations, and the resulting model is a simplified version of what was derived in 5. The model does not include any velocity dependent matrices, which if included could provide a better response. However, the output of these terms would be small due to the velocity $\boldsymbol{\nu} \approx \mathbf{0}$, and would thus only contribute to an increased complexity of the model.

The model is verified through the estimator, as the bias term is small (varies within 2-3 Newton), the modelling error is small, compared to the output of DEN-Mark1. Computational time is a lot faster using the proposed model, as a simulation of 9000 samples takes close to 30 minutes in DEN-Mark1, whereas the same computation with the proposed model only takes around 8 seconds. The ease-to-tune comes from only 3 matrices that needs to be tuned, where $\boldsymbol{M}_{RB}$ and $\boldsymbol{D}_{RB}$ contains terms already measured by FORCE TECHNOLOGY , the time constant matrix $\boldsymbol{T}$ is a function of the two.

A non-linear estimator was developed, based on the works of [FS99]. The estimator includes a linear wave model to filter out the second order wave induced motion, as seen on figure 6.4, the proposed wave-filter removes the second order wave motion from the system. The estimator is based on the derived model, and tuning is therefore easy, the only extra component is the wave frequency ω_o, which are determined from a non-linear fitting to the JONSWAP wave spectrum. The estimator was derived to be exponentially stable, and will thus provide an estimate that converges to the actual value. The bias term $\boldsymbol{b}$ in the estimator expresses unmodelled dynamics, and the size of this term also serves as a measure of the quality of the estimator. Through tests in DEN-Mark1 the bias term have been found to be small even when the vessel cannot hold its position and the thrust input becomes unstable.

The proposed controller utilizes the exponential stability property of the estimator, as $\hat{\boldsymbol{y}} \to \boldsymbol{y}$. The proposed controller includes the wave motion parameter $\boldsymbol{\xi}$, and stability is proven for the controller by designing the two matrices $\boldsymbol{C}_1$ and $\boldsymbol{D}_1$ to be larger than the wave motion matrices of $\dot{\boldsymbol{\xi}}$, this have to the knowledge of the author never been done before. In 8 the non-linear controller have been proven to provide a better response than the linear controller, and the hypothesis stated in the beginning have been proven.

Chapter 10
Discussion

This chapter serves to evaluate the project and discuss possible improvements to the suggested controller. The suggestions have not been implemented, as the main purpose is to develop a controller that is stable in a Lyapunov sense, and the stability calculations are tedious and time consuming.

10.1 Project Discussion

As the current control methodology used at FORCE TECHNOLOGY employs a linear controller to serve as a reference, the proposed could provide far better responses for the system. This does however also have a drawback. The current control configuration provides a very conservative response as to whether the vessel can maintain its position with the thruster configuration, and will thereby guarantee that the actual vessel is able to maintain the position.

An update to this system, would provide better responses, but if the actual ship is fitted with another control system that uses linear techniques, the outcome of the model test might not be realistic, however - this might push the industry in a more non-linear direction.

10.2 Further Improvements

Through the project, possible improvements have been established. They have however not been implemented as some of them are worth an entire study in them selves. This section describes the possible improvement, and briefly discusses a possible solution.

10.2.1 Wave inclusion in the thrust

As the controller currently does not include the wave induced motions, this could be included in the computation of $\boldsymbol{\tau}$. An analysis of the expression yields would change

$\boldsymbol{\tau}$ from the one computed in (7.13) to:

$$\begin{aligned}\boldsymbol{R}(\psi)\boldsymbol{M}^{-1}\boldsymbol{\tau} = &-((\boldsymbol{R}(\psi)\boldsymbol{M}^{-1} + \boldsymbol{R}(\psi)\boldsymbol{S}(r))\hat{\boldsymbol{\nu}} + \boldsymbol{R}(\psi)\boldsymbol{M}^{-1}\boldsymbol{R}^T(\psi)\boldsymbol{K}_2\hat{\mathrm{b}} \\ &+ \ddot{\boldsymbol{y}}_d - (\boldsymbol{C}_1 + \boldsymbol{D}_1)^2\boldsymbol{z}_1 + (\boldsymbol{C}_1 + \boldsymbol{D}_1)\boldsymbol{z}_2 \\ &+ \boldsymbol{z}_1 + (\boldsymbol{C}_2 + \boldsymbol{D}_2)\boldsymbol{z}_2) \\ &+ (\boldsymbol{C}_1 + \boldsymbol{D}_1)(\boldsymbol{C}_w\boldsymbol{A}_w\hat{\boldsymbol{\xi}})\end{aligned} \tag{10.1}$$

However, the proposal would change the stability analysis and are therefore not done in the project. A more tedious study could be carried out to see which terms are *good* and which terms should be removed to have a less fluctuating control signal.

10.2.2 Adaptivity of Controller

Model imperfections should be removed by the bias term $\boldsymbol{b}$ in the estimator. However, to further strengthen the robustness and output of the controller, an adaptive term $\boldsymbol{\theta}$ could be implemented to further remove the model errors, and have a controller that would work on systems with model inaccuracies, and could serve to reduce the time spent tuning the system, as the small model errors would be handled on-line.

[MKK96] suggests a method to include adaptivity in the control strategy. Such an approach could help on the tuning time spent, as the controller would tune itself, within reasonable bounds, and thus ease the tuning procedure.

10.2.3 Input Limitations

The main problem with the controller, is that the non-linear nature of it, allows for rapid changes to the control signal, which is undesirable for ships, as the time constants large, and fast motions are impossible to account for by the actuators. If a limiting term were introduced on $\boldsymbol{\tau}$ that could guarantee to never exceed a certain value, whilst remaining stable, this could prove viable.

The works of [TGT09] shows that such a method could be to implement barrier functions on the input, and penalise the input, and thus effectively saturate it. Allowing it to remain within certain bounds. The bounds could be based on the largest possible thrust deliverable in each direction, such as:

$$\max\{F_x\} = 1550 + 420 + 420 = 2390[\mathrm{kN}] \tag{10.2}$$

$$\max\{F_y\} = 287 + 287 + 287 + 420 + 420 = 1701[\mathrm{kN}] \tag{10.3}$$

$$\max\{M_z\} = 287 l_{stern} - 287 l_{bow1} - 287 l_{bow2} + 420 l_{az-stern}\sin(\frac{pi}{2}) - 420 l_{az_bow}\sin(\tag{10.4}$$

$$frac3\pi 2) = 12144[\mathrm{kNm}] \tag{10.5}$$

This constraint would allow the dynamic range of the input signal to be within actual reach of the individual thrusters, and would also allow the thrust allocation to produce results that were possible to reach. Another factor that could increase robustness, could be to alter the dynamics of the input. Implementing a $\dot{\boldsymbol{\tau}}$ term, and limiting how the rate of change should be on this, could serve to increase the overall result.

This would reduce the wear and tear of the system, as the dynamics of $\boldsymbol{\tau}$ would be slower, as an automatic low pass filtering of the signal would occur. The main purpose of using barrier constraints, is that stability property of the controller can be maintained.

10.2.4 Optimal Thrust Allocation

The thrust allocation should be altered so that it always provides a solution, and to make it more robust. The works of [TAJB04] includes a term to cancel out singularities. The cost function could also be extended to include parameters such as engine wear and tear, the able to change thrust and the dead-zones of the thrusters could be used to improve the response. Dead zones could be used to avoid the Maratos effect, where the thrust is reduced drastically by the water being "sucked" up to the bottom of the vessel.

Another dead-zone would be when the two azimuth thrusters face each other, thus producing thrust that would negate one another, which would be a waste of energy.

10.2.5 Non-linear Wave Model

Instead of using the linear wave model derived in 6.1.1 a non-linear approach to provide a more accurate wave response could be used. This would be more computationally heavy, but theory used to model wind-fields could be applied, as these resemble the wave JONSWAP spectra. The non-linear wave model would provide a more accurate response, but would be computationally more expensive.

An on-line computation of the Response Amplitude Operator (RAO)s could provide the system with almost exact wave responses - this would improve on the estimate $\hat{\mathbf{y}}$, which would reduce fluctuations in the controller, and thus provide a better response.

References

[ALdC98] C. Umeda A.J.P. Leite, J.A.P. Aranha and M.B. de Conti. Current forces in tankers and bifurcation of equilibrium of turret systems: hydrodynamic model and experiments. *Applied Ocean Research*, (20):145–156, 1998.

[Bas61] Willard Bascom. *A Hole In The Bottom of The Sea*. Doubleday & Company, Inc., 1961. Library of Congress Catalog Card Number 61-7638.

[BJMS80] Jens G. Balchen, Nils A. Jenssen, Eldar Mathisen, and Steinar Sælid. A Dynamic Positioning System Based on Kalman Filtering and Optimal Control. *Modeling, Identification and Control*, 1(3):135–163, 1980.

[CJsL12] Rasmus Christensen, Frederik Juul, Nick Østergaard, and Jesper Larsen. Centralized state estimation of distributed maritime surface oceanographers. *Proceedings of the 1st Workshop on Human Centered Robotics*, 1:34–38, 2012.

[FG98] Thor I. Fossen and Aslaug Grovlen. Nonlinear output feedback control of dynamically positioned ships using vectorial observer backstepping. *IEEE Transations on Control Systems Technology*, 6(1):121–128, 1998.

[Fos02] Thor I. Fossen. *Marine Control Systems, Guidance, Navigation and Control of Ships, Rigs and Underwater Vehicles*. Marine Cybernetics AS, 1st edition, 2002.

[Fos11] Thor I. Fossen. *Handbook of Marine Craft Hydrodynamics and Motion Control*. Wiley, 2011.

[FS91] Thor I. Fossen and Svein I. Sagatun. Adaptive control of nonlinear underwater robotic systems. In *In Proceedings of the IEEE International Conference on Robotics and Automation*, pages 1687–1695, 1991.

[FS99] Thor I. Fossen and Jann Peter Strand. Passive nonlinear observer design for ships using lyapunov methods: full-scale experiments with a supply vessel. *Automatica*, 35(1):3–16, 1999.

[GFFEN09] J. David Powell Gene F. Franklin and Abbas Ernami-Naeini. *Feedback Control of Dynamic Systems*. Prentice Hall, 6th edition, 2009.

[Kha02] Hassan K. Khalil. *Nonlinear Systems*. Prentice Hall, 2002.

[Lam95] Horace Lamb. *Hydrodynamics.* Cambridge University Press, 1895.

[MKK96] Ioannis Kanellakopoulos Miroslav Krstic and Petar Kokotovic. *Nonlinear and Adaptive Control Design.* John Wiley & Sons, Inc, 1996.

[NW99] Jorge Nocedal and Stephen J. Wright. *Numerical Optimization.* Springer, 3 edition, 1999.

[SJ83] Steinar Sælid and Nils A. Jenssen. Adaptive ship autopilot with wave filter. *Modeling, Identification and Control*, 4(1):33–45, 1983.

[SNA50] SNAME. Nomenclature for treating the motion of a submerged body through a fluid. Technical report, The Society of Naval Architects and Marine Engineers, 1950. Technical and Research Bulletin No. 1-5.

[TAJB04] Thor I. Fossen Tor A. Johansen and Svein P. Berge. Constrained nonlinear control allocation with singularity avoidance using sequential quadratic programming. *IEEE Transactions on Control Systems Technology*, 12(1):211–216, 2004.

[TGT09] Keng Peng Tee, Shuzhi Sam Ge, and Eng Hock Tay. Barrier lyapunov functions for the control of output-constrained nonlinear systems. *Automatica*, 45(4):918 – 927, 2009.

[Ver12] Det Norske Veritas. Rules for classification of ships, dynamic positioning systems. Technical report, Det Norske Veritas AS, 2012.

[YB98] Chengen Yang and Mogens Blanke. *Rudder-Roll Damping Controller Design using □ Synthesis*, pages 127–132. 1998.

Appendix A
Non-linear Backstepping

This chapter will describe general theory behind integrator backstepping to serve as a reference for the derivation of the controller. Backstepping is based on Lyapunov theory, and bears close resemblance to feedback linearisation. In feedback linearisation all non-linearities are removed, whereas backstepping allows more freedom in the design of the input, and thus allows to keep damping terms, rather than remove them completely, this will be clear throughout this appendix.

This appendix is based on the works of [MKK96] and [Kha02]. Integrator backstepping is motivated by the following proposition A.1.

Proposition A.1. *Consider the system:*

$$\dot{x} = f(x) + g(x)u, \quad f(0) = 0, \tag{A.1}$$

where $x \in \mathbb{R}^n$ is the state and $u \in \mathbb{R}$ is the control input. There exists a continuously differentiable feedback control law

$$u = \alpha(x), \quad \alpha(0) = 0, \tag{A.2}$$

and a smooth, positive definite, radially unbounded function $V : \mathbb{R}^n \to \mathbb{R}$ such that

$$\frac{\partial V}{\partial x}[f(x) + g(x)\alpha(x)] \leq -W(x) \leq 0, \quad \forall x \in \mathbb{R}^n \tag{A.3}$$

where $W : \mathbb{R}^n \to \mathbb{R}$ is positive semidefinite.

In proposition A.1, the choice of input can be designed to remove all non-linearities in (A.1), as in feedback linearisation. However, some non-linearities might prove beneficial to keep. If equation (A.1) contained a quadratic damping term, keeping this might provide better responses than if it was included in the control signal, backstepping allows *good* non-linearities to be kept, whereas the *bad* can be removed. From [MKK96], lemma A.2 is proposed:

Lemma A.2. *Let* (A.1) *be augmented by an integrator.*

$$\dot{x} = f(x) + g(x)\xi \tag{A.4}$$
$$\dot{\xi} = u, \tag{A.5}$$

and suppose that (A.4) *satisfies A.1 with* $\xi \in \mathbb{R}$ *as its control input. (i) If* $W(x)$ *is positive definite, then*

$$V_a(x, \xi) = V(x) + \frac{1}{2}[\xi - \alpha(x)]^2 \tag{A.6}$$

Is a Candidate Lyapunov Function (CLF) for the full system given by (A.4) *and* (A.5)*, that is, there exists a feedback control* $u = \alpha_a(x, \xi)$ *which renders* $x = 0, \xi = 0$ *the Globally Asymptotic Stable (GAS) equilibrium of* (A.4) *and* (A.5)*. One such control input is:*

$$u = -c(\xi - \alpha(x)) + \frac{\partial \alpha}{\partial x}(x)[f(x) + g(x)\xi] - \frac{\partial V}{\partial x}(x)g(x), \quad c > 0 \tag{A.7}$$

(ii) If $W(x)$ *is only positive definite, then there exists a feedback control which renders* $\dot{V}_a \leq -W_a(x, \xi) \leq 0$*, such that* $W_a(x, \xi) > 0$ *whenever* $W(x) > 0$ *or* $\xi \neq \alpha(x)$*. This guarantees global boundedness and convergence of* $[x(t), \xi(t)]^T$ *to the largest invariant set* M_a *contained in the set*

$$E_a = \left\{ \begin{bmatrix} x \\ \xi \end{bmatrix} \in \mathbb{R}^{n+1} | W(x) = 0, \xi = \alpha(x) \right\} \tag{A.8}$$

The theory behind integrator backstepping is easier to understand when illustrated with an example, thus consider the system:

$$f(x, u) = \dot{x} = \cos(x) - x^3 + u \tag{A.9}$$

An easy choice of input, would be to choose u to remove the non-linearities $u = -\cos(x) + x^3 + x$, and thus the remainder is a simple linear system $\dot{x} = x$. Closer examination does however show, that x^3 is negative, and will thus act as a quadratic damping term, hence, a design method that would keep the damping term, and remove the cosine would prove beneficial.

Augmenting (A.9) with an integrator, gives the new system with the virtual state ξ:

$$f(x, \xi) = \dot{x} = \cos(x) - x^3 + \xi \tag{A.10}$$
$$\dot{\xi} = u \tag{A.11}$$

The system (A.10) is depicted on figure A.1.

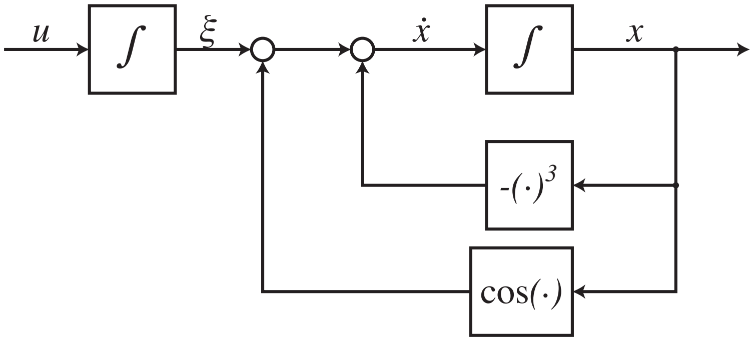

Figure A.1: Depiction of (A.10).

A desired control law ξ for (A.10) with the CLF $V(x) = \frac{1}{2}x^2$ can be defined as:

$$\xi_{desired} = -c_1 x - \cos(x) \triangleq \alpha(x) \tag{A.12}$$

Where $\alpha(x)$ is defined as the stabilizing function for the virtual control ξ. However to achieve that ξ goes to $\xi_{desired}$, the error variable z is defined as the error between the two:

$$z = \xi - \xi_{desired} = \xi - \alpha(x) = \xi + c_1 + \cos(x) \tag{A.13}$$

The whole system is changed to (x, z) coordinates which then re-writes the system in equation (A.10) to:

$$\dot{x} = \cos(x) - x^3 + \xi + c_1 x + \cos(x) - c_1 x \cos(x) = -c_1 x - x^3 + z \tag{A.14}$$

$$\dot{z} = \dot{\xi} - \dot{\alpha} = \dot{\xi} + (c_1 - \sin(x))\dot{x} = u_{backstep} + (c_1 - \sin(x))(-c_1 x - x^3 + z) \tag{A.15}$$

One key feature in backstepping design, is that the stabilizing function $\alpha(x)$ is known, and therefore the derivative thereof is straight forward to compute. Thus, if the input is chosen as:

$$u_{backstep} = -c_2 z - x - (c_1 - \sin(x))(-c_1 x - x^3 + z) \tag{A.16}$$

And a CLF as $V(x, \xi) = \frac{1}{2}x^2 + \frac{1}{2}z^2$, gives the Lyapunov derivative:

$$\dot{(V)} = -c_1 x^2 - c_2 z^2 \tag{A.17}$$

Which indeed is negative definite, as the two integral constants c_1 and c_2 are positive. The augmented system and the corresponding control law is depicted on figure A.2.

The last corraly to menition, is that if the system is a chain of integrators, interpreted as the system has more "layers" - the theory still holds. [MKK96] writes it as the following:

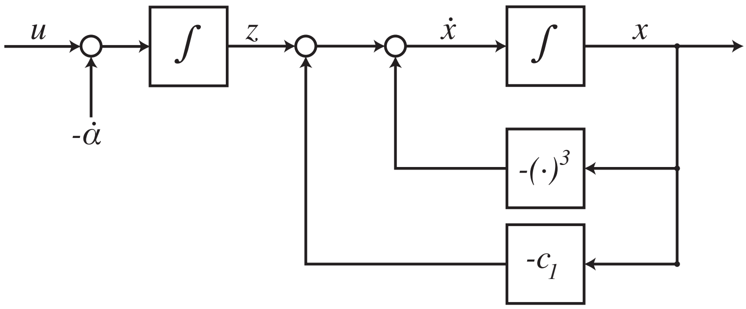

Figure A.2: Depiction of the systems (A.14) and (A.15). The error variable is an integrated difference between the input ξ and the stabilizing function $\alpha(x)$.

Corollary A.3. *Let the system in* (A.1) *satisfying A.1 with* $\alpha(x) = \alpha_0(x)$ *be augmented by a chain of k integrators so that u is replaced by* ξ_1*, the state of the last integrator in the chain:*

$$\dot{x} = f(x) + g(x)\xi_1 \tag{A.18}$$
$$\dot{\xi}_1 = \xi_2 \tag{A.19}$$
$$\vdots \tag{A.20}$$
$$\dot{\xi}_{k-1} = \xi_k \tag{A.21}$$
$$\dot{\xi}_k = u \tag{A.22}$$

For this system, repeated application of A.2 with $\xi_1, \ldots, \xi_k$ *as virtual controls, results in the Lyapunov function:*

$$V_a(x, \xi_1, \ldots, \xi_k) = V(x) + \frac{1}{2}\sum_{i=1}^{k}[\xi_1 - \alpha_{i-1}(x, \xi_1, \ldots, \xi_{i-1})]^2 \tag{A.23}$$

Any choice of feedback control which renders $\dot{V} \leq -W_a(x, \xi_1, \ldots, \xi_k) \leq 0$ *with* $W_a(x, \xi_1, \ldots, \xi_k) = 0$ *only if* $W(x) = 0$ *and* $\xi_i \neq \alpha_{i-1}(x, \xi_1, \ldots, \xi_{i-1}), i = 1, \ldots, k$*, guarantees that* $[x^T(t), \xi_1(t), \ldots, \xi_k(t)]^T$ *is globally bounded and converges to the largest invariant set* M_a *contained in the set* $E_a = \{[x^T, \xi_1, \ldots, \xi_k]^T \in \mathbb{R}^{n+k} | W(x) = 0, \xi_i = \alpha_{i-1}(x, \xi_1, \ldots, \xi_{i-1}), i = 1, \ldots, k\}$*. Furthermore, if* $W(x)$ *is positive definite, that is, if* $x = 0$ *can be rendered GAS through* ξ_1*, then* (A.23) *is a CLF for* (A.18)*, and the equilibrium* $x = 0, \xi = \cdots = \xi_k = 0$ *can be rendered GAS through u.*

This concludes the theory used in the thesis for backstepping.

Appendix B
Vessel Data

System Matrices

The two system matrices for the model of the vessel $\boldsymbol{M}_{RB}$ and $\boldsymbol{D}_{RB}$ are computed to be:

$$\boldsymbol{M}_{RB} = \begin{bmatrix} 0.1089 & 0 & 0 \\ 0 & 0.1975 & 0.8276 \\ 0 & 0.0032 & 0.0057 \end{bmatrix} \tag{B.1}$$

$$\boldsymbol{D}_{RB} = \begin{bmatrix} 0.0077 & 0 & 0 \\ 0 & 0.1191 & -0.0367 \\ 0 & 0.000215 & 3.5524 \cdot 10^{-7} \end{bmatrix} \tag{B.2}$$

These matrices are Bis-scaled. Bis-scaling allows to present the data without the reader being able to interpret the directly, as they are dependent on other factors that are confidential. Bis-scaling of forces and moments are given as:

$$F_{x,Bis} = \frac{F_x}{\mu \rho g \nabla} \tag{B.3}$$

$$N_{\psi,Bis} = \frac{N_\psi}{\mu \rho \nabla L_{pp}} \tag{B.4}$$

$$I_{z,Bis} = \frac{N_\psi}{\mu \rho \nabla L_{pp}^2} \tag{B.5}$$

Where μ is a density ratio, usually defined as 1 for ships or floating structures.

Time Constants

According to [FG98] the time constants of a vessel can be computed from the eigenvalues of the $\boldsymbol{M}_{RB}$ and $\boldsymbol{D}_{RB}$ matrices as:

$$T_i = -\frac{1}{\lambda_i}\sqrt{L_{pp}/g} \tag{B.6}$$

Where λ_i are the eigenvalues of $\boldsymbol{M}_{RB}^{-1}\boldsymbol{D}_{RB}$. Using (B.6) the following time constant matrix is obtained:

$$\boldsymbol{T} = \text{diag}\{51688, 8.513, 73.2126\}[s] \tag{B.7}$$

As all the time constants are positive, the ship is naturally course stable, course stability is depicted on figure B.1.

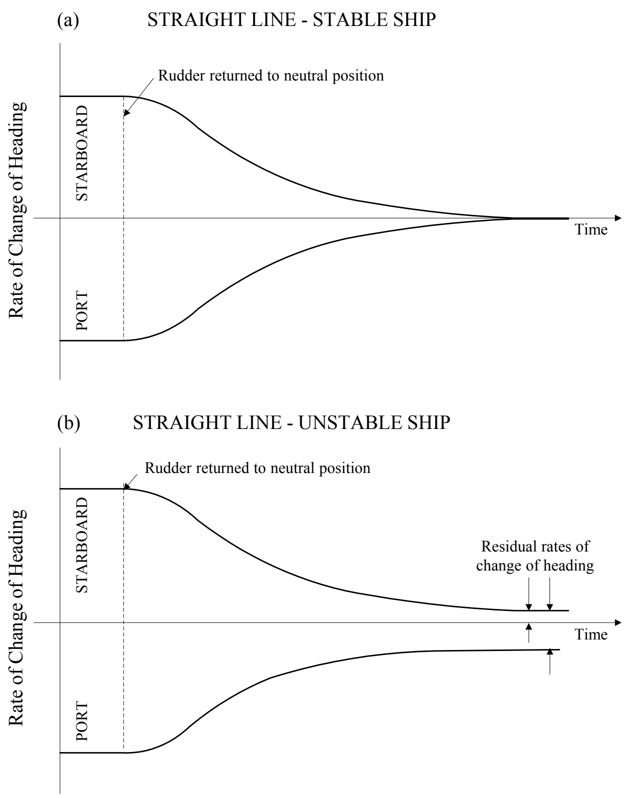

Figure B.1: Depiction of course stability. (a) is a course stable ship, as seen the ship converges towards the original heading, whereas the course unstable ship on (b) continues turning.

Appendix C

Differential Kinematics

The derivative of a rotation matrix is not straight forward to compute, by using the orthogonality of $\boldsymbol{R}(\boldsymbol{\Theta})$ (and for simplicity writing this as $\boldsymbol{R}(t)$), the following can be stated:

$$\boldsymbol{I} = \boldsymbol{R}(t)\boldsymbol{R}^T(t) \tag{C.1}$$

$$\boldsymbol{0} = \dot{\boldsymbol{R}}(t)\boldsymbol{R}^T(t) + \boldsymbol{R}(t)\dot{\boldsymbol{R}}^T(t) \tag{C.2}$$

$$-\boldsymbol{R}(t)\dot{\boldsymbol{R}}^T(t) = \dot{\boldsymbol{R}}(t)\boldsymbol{R}^T(t) \tag{C.3}$$

By using the cross-product operand in (4.8), the following definition is made:

$$\boldsymbol{S}(t) = \dot{\boldsymbol{R}}(t)\boldsymbol{R}^T(t) \tag{C.4}$$

The $\boldsymbol{S}(t)$ in (C.4) can be interpreted as the angular velocities of the system. By using the skew-symmetry of $\boldsymbol{S}$, and isolating for the derivative in (C.3), the derivative can be computed as:

$$\dot{\boldsymbol{R}}(t) = \boldsymbol{R}(t)\boldsymbol{S}(t) \tag{C.5}$$